Removal of aluminum content of concentrated salt solutions by ion exchange: Experimental and simulation study

Benjámin Csorba[1,2], Péter Tóth[2], Andrea Mihalkó[2], László Farkas[2], Renáta Zsanett Boros[2], Iván László Gresits[1*]

[1]Department of Chemical and Environmental Process Engineering, Faculty of Chemical Technology and Biotechnology, Budapest University of Technology and Economics, Budapest, Hungary
[2]BorsodChem Ltd., Kazincbarcika, Hungary
*Corresponding author, e-mail: gresits.ivan@vbk.bme.hu

Received: 31 July 2025; accepted: 6 February 2026

Absract

In the chlor-alkali industry, membrane cell technology requires a significantly purer raw brine than other methods. Further developments of ion exchange for aluminum removal have been required. Several chelating ion exchange resins have been characterized and their Al-binding properties compared. Total binding capacities, breakthrough curves were determined, the effects of pH, temperature, feed brine composition, and column geometry were investigated. Aminomethylphosphonic acid functionalized resins were found to be effective, achieving effluent Al concentrations below 0.01 ppm. At a flow rate of 30 bed volumes per hour and an inlet Al content of 0.5 ppm, a cycle time of up to one month can be achieved. The optimal binding pH is 2.5–3.0, and temperature increase enhances binding efficiency.

Keywords: chlor-alkali industry, aluminum, ion exchange, brine, purification

Tömény sóoldatok alumíniumtartalmának eltávolítása ioncserés eljárással: kísérleti és szimulációs elemzés

Csorba Benjámin[1,2], Tóth Péter[2], Mihalkó Andrea[2], Farkas László[2], Boros Renáta Zsanett[2], Gresits Iván László[1*]

[1]Kémiai és Környezeti Folyamatmérnöki Tanszék, Vegyészmérnöki és Biomérnöki Kar, Budapesti Műszaki és Gazdaságtudományi Egyetem, Budapest, Magyarország
[2]BorsodChem Zrt., Kazincbarcika, Magyarország

Összefoglalás

A klór-alkáli iparban a korábban elterjedt higanykatódos elektrolízist napjainkra a környezetbarátabb és gazdaságosabb, jelenleg a klórgyártás legjobb elérhető technológiájának (BAT) minősülő membráncellás módszer váltotta fel. Ezen technológia azonban jóval tisztább, fémszennyezőket (jellemzően Mg, Ca, Sr, Ba, Al, Fe) legfeljebb ppb (milliárdodrész, tömegre vetítve) nagyságrendben tartalmazó sólevet igényel. Míg az alkáliföldfémek eltávolításával számos szerző foglalkozott, az alumínium eltávolítása további fejlesztéseket igényelt. Munkánkban ezen fém ioncserés eltávolításának kísérleti és szimulációs vizsgálatával foglalkoztunk.

Kísérleteinkhez több különböző gyártótól származó, különböző funkciós csoportokkal rendelkező ioncserélő gyantákat használtunk, melyeket karakterizáltuk. Vizsgáltuk az egyes gyanták teljes Al-megkötő kapacitását, és annak pH-függését is. Ez alapján az aminometilfoszfonsav funkciós csoportú gyanták Al-megkötő kapacitása 0,65–0,71 mol/L (nedves, Na^+ formájú gyanta halmaztérfogatára vonatkoztatva), az optimális pH 2,5–3,0. Ezen tartomány jelentősen eltér az alkáliföldfémek iminodiacetát gyantával történő megkötésének optimális pH-tartományától, így a két megkötési cél egyazon oszlopban, kevert gyantaággyal nem valósítható meg, az alumínium eltávolításához külön ioncserélő oszlop szükséges.

A jellemző üzemi körülményeket jól modellező folyamatos megkötési kísérleteket is végeztünk, vizsgálva a hőmérséklet, az oszlopgeometria, a belépő sólé-összetétel és a gyanta telítettségi fokának hatását. Az eltávolítási hatékonyság a hőmérséklet emelésével jelentősen javult, a klór-alkáli iparban jellemző 60 °C hőmérsékleten 0,01 ppm alatti végső Al-koncentráció is elérhető volt. A BAT-beli kilépő Al-koncentrációlimitet figyelembe véve 50% feletti kapacitáskihasználás is megvalósítható volt. A gyantaágy geometriájának és a további jellemző fémszennyezők jelenlétének nem volt jelentős hatása.

Az ioncsere folyamatát a Homogén Felületi Diffúzió Modellje (HSDM) alkalmazásával is vizsgáltuk, kísérleti adataink alapul vételével. A szimuláció során a méretnövelés megvalósíthatónak bizonyult, 30 BV/h sóléáram (30-szoros gyantaágy-térfogatnak megfelelő sólé átáramlása óránként) és 0,5 ppm belépő Al-koncentráció mellett akár 1 hónapos ciklusidő is elérhető volt. Vizsgáltuk a sóléáram, a belépő Al-tartalom, a gyanta mennyiségének és a gyantaágy geometriájának hatását is, felvéve áttörési görbéket, izoplánokat és izokronokat. Ez alapján a rendszer áttörése a belépő Al-tartalom időszakos megemelkedésekor sem következik be jelentősen korábban, a gyantaágy geometriájának nincs jelentős hatása, és az eltávolítás még 60 BV/h térfogatáramnál is hatékony, azonban rövidebb ciklusidő mellett.

Eredményeinket felhasználva Magyarország klór-alkáli iparágának vezető vállalata, a BorsodChem Zrt. új, 13 m^3 aminometilfoszfonsav csoportú gyantát tartalmazó ioncserélő oszlopot telepített mindkét membráncellás üzemébe, melyek megfelelő üzembiztonsággal üzemelnek.

Kulcsszavak: klór-alkáli ipar, alumínium, ioncsere, sólé, tisztítás

Introduction

The industrial production of chlorine is generally based on the electrolysis of sodium chloride (NaCl) solution, which yields hydrogen gas and sodium hydroxide (NaOH) solution as co-products *(Fauvarque 1996)*. These are all essential raw materials in the chemical industry *(Stringer–Johnston 2001)*, with wide-ranging applications such as PVC production, polyurethane synthesis *(Ding et al. 2013)*, ammonia synthesis *(Humphreys–Lan–Tao 2021)*, petroleum refining, and the manufacture of cleaning agents *(Brée et al. 2020)*. Mercury cell electrolysis was previously widespread; however, due to the environmental hazards associated with mercury use *(Ogunbiyi et al. 2021; Sola et al. 2020)*, this technology has been phased out in most countries in accordance with the Minamata Convention *(Feng et al. 2022; Minamata Convention on Mercury 2021; Selin et al. 2018)*, and has been largely replaced by membrane cell electrolysis. This latter is now considered the Best Available Technique (BAT) for chlorine production, offering both economic and ecological advantages over mercury and diaphragm cell methods *(European Commission 2014; Margallo et al. 2016; Pátzay–Tungler–Mika 2011)*.

Nonetheless, an important engineering challenge has emerged: membrane cell technology requires a significantly purer brine as feedstock, with metal contaminants present only in the parts-per-billion (ppb, by mass) range. The combined concentration of Ca and Mg must not exceed 20 ppb; for Sr, the limit is 40 ppb; for Ba, 50 ppb (if the sulfate concentration exceeds 6 g/L); for Fe, 1 ppm; for Ni, 10 ppb; for other heavy metals, 100 ppb; and for aluminum, likewise 100 ppb. However, under conditions of full membrane utilization, some membrane manufacturers may specify even stricter limits *(European Commission 2014; Schmittinger et al. 2012)*.

Even at sub-mg/kg concentrations, metallic impurities – particularly aluminum – can severely damage the cell membranes. This leads to reduced lifespan of the costly electrolysis membranes, contamination of the products (e.g., brine permeation contaminates the NaOH, while increased oxygen evolution due to undesired side reaction contaminates the chlorine gas), and an increase in specific energy consumption *(European Commission 2014; Ramírez–Cisternas–Kraslawski 2017)*. In addition, damage to the membrane is also detrimental to operational safety. Therefore, appropriate brine purification is of critical importance from both economic and sustainability perspectives.

The typical concentrations of metallic impurities in sea salt are as follows: 1.1–1.3 wt% Ca, 3.6–4.1 wt% Mg, 230–250 ppm Sr, 0.5–0.7 ppm Ba, 10–30 ppb Al, 0.1 ppm Fe, and 80–90 ppm Si *(Anthoni 2006; Hydes 1979; Le Bihan et al. 2003; Millero et al. 2008)*. By contrast, rock salt typically contains significantly higher levels of aluminum – up to 93 ppm – and iron – up to 157 ppm – contamination compared to sea salt. Although the content of alkaline earth metals is generally lower in rock salt, these species still represent the primary impurities in this case *(Binega 2006; Titler–Curry 2011)*.

During purification, poorly soluble hydroxide or carbonate salts are formed under alkaline conditions from Fe^{3+}, Ca^{2+}, and Mg^{2+} ions. These precipitates can then be removed by sedimentation and filtration. The rest of metal ions are typically removed by ion exchange. At this final stage of the purification process, achieving the BAT threshold values becomes critically important *(European Commission 2014)*.

Among the metallic impurities to be removed, aluminum – classified as an amphoteric metal – exhibits the most complex solution chemistry *(Hem–Roberson 1967; Rubin–Hayden, 1973)*. The literature on aluminum solution chemistry in concentrated saline environments is limited.

Aluminum exhibits extremely low solubility in neutral solutions, with a solubility minimum at approximately pH 6 under ambient conditions *(Rubin–Hayden, 1973)*.

Moving away from this pH in either direction results in an increase in solubility. The poor solubility of aluminum around pH 6 constitutes an important design constraint and limiting factor in ion exchange experiments, as the formation of precipitates must be avoided.

Most publications and patents in related fields focus on the removal of water hardness–causing ions (Ca^{2+}, Mg^{2+}), as well as Ba^{2+}, Sr^{2+}, Fe^{3+}, Mn^{2+}, and various heavy metals by ion exchange *(Blokhin–Murashkin–Mikhaylenko 2021; Chidambaran–Bisht–Raina 2014; European Commission 2020; Kiefer–Höll 2001; Kurkinen–Virolainen–Sainio 2021; Marcin–Sage 2017; Namana et al. 2024; Wallace 2015, 2021)*. For this purpose, weakly or strongly acidic cation exchange resins or chelating resins are typically employed. Regeneration is generally performed using acids, most commonly hydrochloric acid. Alkali is used only for post-regeneration neutralization or to convert the resin into its sodium form. In contrast, Li and co-workers *(Li et al. 2016)* applied a strongly acidic resin with sulfonic acid functional groups (Purolite C145), where Al^{3+} ions are used to displace the less selectively bound *(Cséfalvay et al. 2012)* divalent alkaline earth metal ions during the regeneration phase.

According to US Patent 10,954,150 B2 *(Wallace 2021)* and 2015/077,727 A1 *(Wallace 2015)*, an ion exchange resin of the Amberlite IRC-747 type, bearing aminophosphonic acid functional groups, can be used to remove alkaline earth metal ions under mildly basic conditions (pH 8–9). The applicability of this resin is also mentioned as an example in US Patent 9,719,179 B2 *(Marcin–Sage 2017)*. According to manufacturer recommendations, iminodiacetic resins (see structure in *Figure 1*) are commonly used for the purification of brine solutions in membrane cell electrolysis, targeting Ca^{2+}, Mg^{2+}, Ba^{2+}, Sr^{2+}, and Fe^{3+} impurities. This is explicitly stated in the technical datasheet of the Lewatit MonoPlus TP 208 resin. However, this resin is not explicitly recommended for the removal of Al^{3+} ions *(LANXESS Deutschland GmbH 2024)*. Furthermore, industrial experience and previous measurements by BorsodChem Ltd. have demonstrated that operation in compliance with BAT limit values is reliably achieved for alkaline earth metals and iron employing iminodiacetic resin, without further development *(Tamás 2021)*.

Numerous ion exchange procedures for aluminum binding are reported. However, in many cases, the aim was not to achieve the lowest possible final aluminum concentration, but rather to separate and concentrate aluminum as completely as possible. Therefore, the reported efficiencies are often not relevant to our case. Das and Pobi *(1991)* used an ion exchange resin functionalized with N-benzoylphenylhydroxylamine, with an optimal pH of 2.5. Wong and Dudeney *(1991)* applied a strongly acidic (sulfonate-functionalized) cation exchange resin (Amberlite IR 120) to remove aluminum, with binding enhanced by the presence of ammonia. However, the aluminum concentration in the solution did not drop below 260 mg/L.

Petrie et al. *(1984)* employed a strongly basic anion exchange resin in the chloride form (Amberlite IRA400) for aluminum removal from dialysis fluids at near-neutral pH. The resin was used in a mixed bed with cation exchange resin, enabling aluminum removal and water softening in a single technological unit. The anion exchange resin was regenerated using concentrated sodium chloride solution. Although the method was highly effective for aluminum removal, even achieving BAT-compliant final concentrations (as low as 5.1 µg/L in the most favorable case), this method could not be considered in our case, as the solution to be treated already contains concentrated sodium chloride. Horton and Thomason *(1956)* also used a strongly basic anion exchange resin (Dowex 1, chloride form).

Nye et al. *(1961)* utilized montmorillonite and kaolinite, materials with ion exchange properties, to remove aluminum. Costa, Silva and Vieira *(2021)* investigated aluminum removal using residual biomass obtained during alginate extraction from *S. filipendula* brown algae as a biosorbent. The material acted via cation exchange and primarily contained carboxylic acid, sulfonic acid, and amino functional groups.

Virolainen et al. *(2021)* employed an ion exchange resin functionalized with aminomethylphosphonic acid groups (structure shown in *Figure 1*; Lewatit TP260) for the removal of Al^{3+}, Fe^{3+}, Mn^{2+}, and Cu^{2+} from solutions obtained from the leaching of lithium-ion batteries. Compared with iminodiacetate, sulfonic acid, and carboxylic acid functionalized resins, this method proved highly effective for aluminum removal at 60 °C, with an optimal pH of 3. However, the initial aluminum concentration in their study was 1.3 g/L – three orders of magnitude higher than the starting concentration in our brine solution and four to five orders of magnitude above the target limit – thus, direct conclusions are difficult to draw.

Aminomethylphosphonic acid is a multivalent organic acid with pKa values of 1.45, 5.4, and 11.0. In the first two steps, the hydrogen atoms of the OH groups bonded to the phosphorus are released, followed by the proton that contributes to the partial positive charge on the nitrogen atom. In chelation, the non-bonding electron pairs on the oxygen ligands attached to phosphorus are involved *(Sraidi et al. 2024)*.

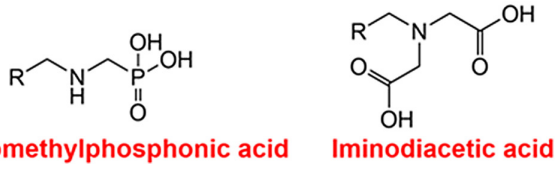

Aminomethylphosphonic acid Iminodiacetic acid

Figure 1 The structure of aminomethylphosphonic acid and iminodiacetic acid. The connection to the polymer that forms the support of the resin is marked R

Source: Own work

In addition to the aforementioned aluminum removal, ion exchange resins functionalized with aminomethylphosphonic acid groups can be employed for a variety of other purification purposes, for example removal of F^- ions *(Popat–Anand–Dasare 1994)*, Li^+ ions *(Çiçek–Yilmaz–Arar 2018, Recepoğlu 2024)*, Cu^{2+}, Ni^{2+}, Cd^{2+}, Zn^{2+}, Co^{2+} ions *(Kiefer–Höll 2001)*, and rare earth elements *(Sraidi et al. 2024)*. It was found that the presence of Al^{3+} ions negatively affected the binding of rare earth elements when using Lewatit TP260, suggesting that aluminum binds more favorably than the studied rare earth metals *(Hérès et al. 2018)*. Hermassi et al. *(2021)* also investigated the binding of rare earth elements and aluminum using Lewatit TP260 under acidic conditions. Contrary to the results of previously mentioned authors, for Al^{3+} ions, starting from a concentration of 375 mg/L, the observed binding was minimal, with only 7% removal efficiency.

None of the identified patents deal with aluminum removal using ion exchange resins functionalized with aminomethylphosphonic or iminodiacetic acid groups. However, two patents *(Jie–Yonggao 2021a, 2021b)* investigate aluminum removal by ion exchange using strongly acidic cation exchange resins in a highly similar way. During the sorption phase, a flow rate of 1–5 bed volumes per hour (BV/h) is applied – this unit is commonly used in ion exchange operations and expresses the hourly volume of liquid passed through the resin bed relative to the bed volume. The aluminum content in the effluent is below 5 mg/L. The resins are regenerated using 3–10 wt% sulfuric acid solution. Similar procedure is applied in U.S. Patent No. US 2023/0,050,044 A1 *(Liu et al. 2023)*.

Ultimately, we decided to employ both iminodiacetate and aminomethylphosphonic acid functionalized resins.

Detailed simulation of ion exchange processes requires specialized software. In the scientific literature, examples can be found for the use of programs such as Aspen Adsorption *(Gallindo et al. 2021; Mc Lein Roger et al. 2023)* and Aspen Chromatography *(Venkatesan–Wankat 2011)*, as well as custom-developed, theoretically well-founded code created by researchers themselves *(Franco et al. 2013; Ma et al. 2019; Vo–Shallcross 2003)*.

Gallindo et al. *(2021)* studied the removal of Zn^{2+} ions using a zeolite-based ion exchange process and the Aspen Adsorption software. Required input data included Langmuir constants describing the sorption process, porosity data, particle diameter and pore volume of the adsorbent, as well as solution density and viscosity. They used the ELECNRTL (eNRTL) thermodynamic model, which is also suitable for describing concentrated saline solutions *(Chen et al. 1982; Chen–Evans 1986; García et al. 2019; Fengmin et al. 2018; Hossain–Bhattacharia–Chen 2016; Hossain et al. 2018; Kirkes–Saravi–Chen 2021; Song–Chen 2009; Wang et al. 2022)*. The sorption process was modeled using an interfacial mass transfer model, and intraparticle mass transport was described by diffusion. Venkatesan and Wankat *(2011)* simulated seawater softening by ion exchange using Aspen Chromatography. Among the required inputs were solution density and viscosity, resin particle density and capacity, Ca/Na and Mg/Na selectivity coefficients, porosity values, axial dispersion coefficients, and mass transfer coefficients. The simulation involved a few simplifications: constant pressure and flow rate along the column, constant selectivity coefficient, and neglect of axial dispersion and other potential non-ideal effects.

Ma et al. *(2019)* investigated the removal of Ni^{2+} ions from wastewater by an iminodiacetate-functionalized resin in a mixed ionic form (partially H^+ and partially Na^+ form) using a custom-developed simulation program. The program describes the intraparticle processes using the Homogeneous Surface Diffusion Model (HSDM). They found that the HSDM is highly suitable for partially replacing costly pilot-scale experiments when applying chelating resins in fixed-bed configurations, significantly reducing the time required during process design. The model is based on a mechanism in which adsorption occurs on the outer surface of spherical resin beads, followed by diffusion into the interior of the resin. According to the model, the driving force for mass transfer through the external film on the resin bead surface is the linear concentration gradient. The program first solves the partial differential equations describing intraparticle diffusion for the resin phase using the Crank–Nicolson algorithm, which is based on the finite difference method. Based on experimentally provided Langmuir constants used as input parameters, it then calculates the surface liquid-phase concentration, followed by solving the partial differential equations for the liquid phase. The simulation operates with three running indices: radial position within the resin bead, column height, and time. During the computation, the internal diffusion coefficient of the resin particles is optimized – that is, the simulation runs until the calculated results match the experimental data as closely as possible, by minimizing the sum of squared errors (SSE). Ultimately, this study was chosen as the basis for developing our own simulation program.

The investigations were conducted in a real industrial environment in cooperation with BorsodChem Ltd., Hungary's leading chlorine manufacturer, thereby allowing the possibility for laboratory findings to be implemented on an industrial scale. During problem assessment, it was identified that the most critical issue in the company's case was the aluminum content of the brine, which, at the beginning of the project, deviated the most from the BAT reference values. A key novelty of the present research lies in the fact that, while other authors have typically focused exclusively on the removal of alkaline earth metal ions, special emphasis has been placed on the removal of aluminum ions from concentrated salt solutions by us.

Experimental methods

The following chemicals were supplied by VWR International: eriochrome cyanine R (ECR, pure), calmagite (indicator grade), ethylene glycol-bis(β-aminoethyl ether)-N,N,N′,N′-tetraacetic acid (EGTA, ≥98.5%), 3-(N-morpholino)propanesulfonic acid (MOPS, ultra pure – >98.5%), NaCl (99.9%), $CaCl_2 \cdot 2\ H_2O$ (97.0–103%), $MgSO_4 \cdot 7\ H_2O$ (>99.5%), $FeCl_3 \cdot 6\ H_2O$ (99.0–102%), ammonia solution (analytical grade), solid aluminum (99.8%), cetyltrimethylammonium bromide (CTAB, >99%), hydrochloric acid solution (analytical grade), NaOH (98.0%), formic acid (≥99%), acetic acid (99.9%), and sodium acetate trihydrate ($CH_3COONa \cdot 3H_2O$, 100.0%). The ion exchange resins were obtained from suppliers of the Chlorine Plant of BorsodChem Ltd. All chemicals were used without further purification.

In addition, brine purified using the current industrial technology of BorsodChem Ltd. was used; its composition was determined prior to application. In the following sections, solutions prepared from laboratory-grade reagents will be referred to as Model 1, while solutions based on the above-mentioned industrially purified concentrated brine and laboratory-grade stock solutions and buffer solutions will be referred to as Model 2. The aluminum stock solution was prepared by dissolving solid metallic aluminum in hydrochloric acid. Other stock solutions were prepared by the dissolution of $CaCl_2 \cdot 2\ H_2O$, $MgSO_4 \cdot 7\ H_2O$ or $FeCl_3 \cdot 6\ H_2O$ in water. Distilled water was produced by us.

Spectrophotometric measurements were performed using an Analytikjena Specord® 210 Plus ultraviolet-visible (UV-VIS) spectrophotometer (Jena, Germany; absorbance measurement accuracy: 0.0001). During the experiments, pH and temperature were measured using a Mettler Toledo FiveEasy instrument (Columbus, Ohio, USA; measurement accuracy: ±0.01 for pH and ±0.1 °C for temperature). Mass measurements were conducted using a Sartorius Quintix224-1 CEU analytical balance (Göttingen, Germany; accuracy: 0.1 mg). Temperature control was achieved using a Julabo MV-4/KUE thermostat (Seelbach, Germany; accuracy: 0.1 °C). The specific surface area of the ion exchange resins was determined using a Quantachrome Autosorb iQ gas adsorption analyzer, while the dynamic viscosity of concentrated NaCl solutions was measured using a Brookfield Metek DVNext viscometer.

Characterization of ion exchange resins

The characterization of individual ion exchange resins – namely the collection and determination of their most important physical and chemical properties – is essential for interpreting the results of experiments. Furthermore, certain parameters are also required as input for modeling and simulation. Some data were obtained from the manufacturers' datasheets, while others were determined by measurements or calculated from manufacturer data. Detailed descriptions are provided in the Appendix.

Investigation of resin capacity, effect of pH

The experimentally tested resins were as follows:

- Resin with aminomethylphosphonic acid functional groups from an Asian manufacturer
- Resin with aminomethylphosphonic acid functional groups from a European manufacturer
- Resin with iminodiacetate functional groups from an Asian manufacturer
- Resin with iminodiacetate functional groups from a European manufacturer

During the capacity tests, 10 mL of resin (previously regenerated twice using the following sequence: rinse with water, regeneration with 6.0 wt% aqueous HCl solution, rinse with water, regeneration with 5.2 wt% aqueous NaOH solution, rinse with water) was mixed in 200 g of 25 wt% Model 1 NaCl solution at room temperature using a shaker. Aluminum was added to the solution using an $AlCl_3$ stock solution, and the residual aluminum content in the solution was periodically measured using our developed photometric method *(Csorba et al. 2023, 2024)*. When the aluminum concentration dropped near the detection limit, further amount of the aluminum stock solution was added. Once the aluminum concentration in the solution stabilized, the amount bound to the resin was calculated using a mass balance equation, from which the resin capacity was derived.

When dosing the aluminum stock solution, care was taken to ensure that the resulting aluminum concentration in solution remained below its solubility limit, to avoid counting any precipitated aluminum as sorbed aluminum. To achieve this, previous solubility studies served as a reference. The pH-dependence of capacity was examined in brine solutions adjusted to various pH values. For pH adjustment, hydrochloric acid was used up to pH 2, a formic acid–sodium formate buffer between pH 2 and 4, ammonia–ammonium chloride buffer at pH 9 and 10, and NaOH solution at pH 11. The pH was continuously monitored and adjusted as needed.

Unfortunately, no capacity measurements could be performed near neutral pH, as the low solubility of aluminum would have required either hundreds of kilograms of brine to saturate the expected capacity, or – in the case of using smaller brine volumes – saturation of the 10 mL resin volume would have required several hundred dosing steps.

Static kinetic investigation of metal ion sorption by ion exchange

The time course of the sorption process was investigated using batch-shaking experiments. For this purpose, the

resins were saturated to varying degrees (based on their measured capacities) using calculated amounts of aluminum stock solution, in a manner similar to that used in the capacity measurements. The saturation process was continued until at least 99% of the added aluminum – based on our photometric analysis – was bound by the resin. The resins were then contacted with fresh 25 wt% Model 1 NaCl solution containing 1 ppm aluminum. Samples were taken at defined time intervals, and the residual aluminum concentration in solution was measured. The pH was adjusted to 3 by formic acid–sodium formate buffer, which had previously been identified as optimal in the capacity tests.

These experiments were primarily conducted at room temperature. However, in the most promising cases, the experiments were also repeated at 60 °C. Under industrial conditions, the residence time of brine in ion exchange columns is typically in the order of a few minutes. Therefore, our aim was to reduce the aluminum content to below 0.05 ppm within a few – ideally no more than 10–20 – minutes even at room temperature.

For resins with iminodiacetate functional groups, the experiment was also performed for magnesium binding, using iminodiacetic resins from two different manufacturers. In these tests, fully regenerated resins were used, and the effect of pH was studied over the range of pH 3 to pH 9 using formic acid–sodium formate buffer at pH 3, acetic acid–sodium acetate buffer at pH 5, MOPS–NaOH buffer at pH 6, 7 and 8, and ammonia–ammonium chloride buffer at pH 9. The residual magnesium content in solution was determined using our adapted photometric method.

For the determination of reaction rate constants overall mass transfer coefficients, the results of experimental series conducted at both room temperature and 60 °C were used, specifically those in which the resin was initially unsaturated. The physicochemical and mathematical background of the mass transfer coefficient determination is described in detail in the Appendix. The calculations are based on the transport equation describing component transfer.

Dynamic investigation of Al^{3+} ion sorption by ion exchange

In the time-consuming dynamic sorption experiments, aminomethylphosphonic acid functionalized resins were used, previously identified as optimal in the preceding sections, under their optimal pH (2.5–3). Temperatures ranged from 20 to 80 °C. Prior to entering the resin bed, the brine was passed through a heat exchanger, and the resin column itself was thermostated accordingly.

During the experiments, the aluminum concentration of the Model 2 brine was adjusted to 0.5 ppm. This solution was then continuously passed through a 30 mL resin bed at a flow rate of 30 BV/h, a value matching current industrial practice. Decreasing this flow rate would only be possible through major investment (e.g., larger columns), while increasing it is neither necessary nor justified.

The resin was pre-regenerated before each run. In some cases, it was preloaded with aluminum to various degrees of saturation (as also applied in the kinetic studies), in order to observe the outlet aluminum concentration at different levels of saturation – effectively recording simplified breakthrough curves. The steady-state aluminum concentration in the effluent was determined using our developed photometric method.

Under these operational parameters, full saturation breakthrough tests could not be carried out due to practical constraints. Considering the resin capacity, the inlet flow rate, and the aluminum concentration of the feed, a single full experiment would require approximately 1,000 hours – equivalent to about half a year assuming 8-hour workdays. Performing such experiments with significantly higher inlet concentrations would be unjustified, as they would not reflect the parameters encountered in chlor-alkali industry practice.

In addition, the effect of column geometry was also investigated. The experimental conditions remained as described above, with the exception that 25 mL of resin was used and the columns were replaced between runs to vary the height-to-diameter ratio while keeping the resin volume constant.

Furthermore, at 60 °C and 40% saturation, the effect of the presence of other metal impurities (1.5 ppm Fe, 5 ppm Mg, and/or 300 ppm Ca) on aluminum sorption efficiency was examined. Such contamination could occur under industrial conditions if the ion exchange columns upstream of the aluminum removal stage are not functioning properly.

Assuming that equilibrium is approximately established between the resin phase and the solution phase during flow, the obtained results can be used to determine the constants of adsorption isotherms that describe ion exchange as an adsorption process. During each dynamic sorption run, the saturation level of the resin phase changes only slightly (by at most a few tenths of a percent), thus the resin phase concentration can be regarded as constant. The solution-phase concentration was measured directly. However, in order to apply adsorption isotherms, the concentrations must be converted: for the resin phase to mol/kg (based on wet, H^+ form resin particle volume), and for the solution phase to mol/dm³. These conversions are based on the characterization data obtained for the ion exchange resins.

Several types of isotherms are described in the literature *(Kiefer–Höll, 2001; Ma et al. 2019)*. Among them, the BET isotherm was deemed unsuitable for describing the equilibrium relationship in this case, since multilayer adsorption is not expected due to the ion exchange mechanism. Instead, the applicability of the Langmuir

isotherm and its modified forms were tested. The general form of the Langmuir isotherm is as follows *(Cséfalvay et al. 2012: 825)*:

$$\frac{q}{q_{\max}} = \frac{K \cdot c}{1 + K \cdot c} \text{ or } q = \frac{K' \cdot c}{1 + K \cdot c}, \text{ where } K' = K \cdot q_{\max}$$

Here, q denotes the instantaneous aluminum concentration in the resin phase, q_{max} represents the total aluminum-binding capacity of the resin, c is the aluminum concentration in the brine that is in equilibrium with the resin, and K is the equilibrium constant of the binding reaction.

In their ion exchange studies, Ma and co-workers identified the Redlich–Peterson isotherm as the most suitable model *(Ma et al. 2019)*. This isotherm can be described using an equation structurally similar to the Langmuir isotherm:

$$\frac{q}{q_{\max}} = \frac{K \cdot c}{1 + a \cdot c^b} \text{ or } q = \frac{K' \cdot c}{1 + a \cdot c^b}, \text{ where } K' = K \cdot q_{\max}$$

In addition to the equilibrium constant, the selectivity and the distribution coefficients are also calculated. The selectivity coefficient is described by the following equation *(Cséfalvay et al. 2012: 375)*:

$$T = \frac{y \cdot (1 - x)}{x \cdot (1 - y)},$$

where y is the equivalent fraction of aluminum in the resin phase, and x is the equivalent fraction in the liquid phase. The distribution coefficient is defined as the ratio of the aluminum concentration in the resin phase to that in the liquid phase, both expressed in mol/dm^3.

The selectivity and the distribution coefficients at 20 and 60 °C are calculated for data points where the aluminum concentration measured in the brine exceeded the detection limit, and then averaged.

Analytical methods

The aluminum content was determined using our developed spectrophotometric method *(Csorba et al. 2023, 2024)*. As the complexing reagent, a 0.08000 wt% ECR solution adjusted to pH 2.9 with acetic acid was applied. This solution was prepared by weighing a known amount of solid ECR, dissolving it in water while adjusting the pH to 2.9 by adding acetic acid dropwise, and then diluting the solution with distilled water to the desired final concentration. To enhance the absorbance peak, CTAB in a 0.546 wt% solution was added, which was also prepared by weight. The buffers, included in the CTAB-containing solution, consisted of 35.8 wt% sodium acetate trihydrate ($CH_3COONa \cdot 3H_2O$) and 2.37 wt% acetic acid.

The measurement procedure was as follows:

- Added ECR solution to the sample in a mass ratio of 1:6 (reagent to sample).
- Added CTAB-containing buffer solution to the system in a mass ratio of 1:3 based on the initial sample mass.
- Measured the absorbance of the sample 15–90 minutes after mixing. Using the dilution factor and the calibration curve prepared for the specific salt concentration of the sample, the dissolved aluminum concentration could be determined.

A spectrophotometric method suitable for magnesium determination was developed by adapting the method of Ingman and Ringbom *(1966)* to high-salt matrices, using calmagite and EGTA. For the photometric measurement, the pH of a 10.0 g brine sample was adjusted to 12.2–12.3 using NaOH solution, and the total mass was brought to 11.0 g with distilled water to ensure consistent dilution across all samples and calibration standards. Then, 1.0 g of 0.001 M EGTA solution was added to mask any calcium content, followed by 1.0 g of 0.0025 M calmagite solution. EGTA and calmagite were also added to the blank sample, as both reagents influenced absorbance even in the absence of calcium. Absorbance was measured after a 30-minute waiting period, and the concentration was calculated using the calibration curve recorded in the 0.03–1 ppm Mg concentration range, together with the applied dilution mass ratio.

In our experience, the calmagite solution has very poor stability and loses its effectiveness within 24 hours, even when stored in a refrigerator. Therefore, it is advisable to prepare a fresh calmagite solution and corresponding calibration curve each day before starting measurements.

Results and discussion

Characterization of ion exchange resins

A number of parameters related to the aminomethylphosphonic ion exchange resins were required. These data are listed in *Table 1*. Some of them were available from the manufacturers' technical datasheets. Additional parameters calculated based on these data, and further missing parameters were determined experimentally, according to the Appendix.

Based on *Table 1*, it can be observed that the ion exchange resins with aminomethylphosphonic acid functional groups, originating from two different suppliers, are largely similar; however, significant differences were found in average particle size and uniformity coefficient. The resin from the European supplier exhibited a markedly smaller average particle size and a more homogeneous size distribution, as indicated by a uniformity coefficient close to 1. The uniformity coefficient is defined as the ratio of the particle diameters at which 60% and 10% of the sample mass is finer.

Table 1 | Data for aminomethylphosphonic acid functional group resins

Data from the manufacturers' datasheets	European manufacturer	Asian manufacturer
Effective size / mm	0.55–0,6	0.4–1.25
Bulk density, wet, Na^+ form (ρ_{bulk}) / kg/m^3	720	750
Particle density, wet, Na^+ form ($\rho_{particle}$) / kg/m^3	1180	1170
Moisture content / wt%	58–62	55–65
Average particle diameter, wet, Na^+ form / mm	0.63	
Uniformity coefficient	<1.1	
Data derived by calculation from manufacturers' datasheets	**European manufacturer**	**Asian manufacturer**
External porosity (ε_{out})	0.39	0.36
Pore volume, wet, Na^+ form (V_{pore}) / cm^3/g	0.60	0.60
Internal porosity (ε_{in})	0.71	0.70
Solid density, Na^+ form (ρ_{true}) / kg/m^3	1620	1570
Data obtained from laboratory measurements	**European manufacturer**	**Asian manufacturer**
Particle density, wet, H^+ form ($\rho'_{particle}$) / kg/m^3	1420	1460
Solid density, H^+ form (ρ'_{true}) / kg/m^3	2440	2540
Average particle diameter, wet, H^+ form / mm	0.58	0.91
Average particle diameter, dry, H^+ form / mm	0.43	0.67
Average particle diameter, wet, Na^+ form / mm		0.99
Pore volume, wet, H^+ form (V'_{pore}) / cm^3/g	0.50	0.48
Volume reduction during $Na^+ \rightarrow H^+$ conversion / %	20	23
Specific surface area by volume of resin bed, wet, H^+ form / m^2/m^3	$1.55 \cdot 10^7$	$1.45 \cdot 10^7$
Specific surface area by weight of resin, wet, H^+ form / m^2/g	17.8	15.5

Source: Own work

Comparison of the aluminum binding capacity of ion exchange resins, effect of pH

The Al-binding capacity values measured for the aminomethylphosphonic acid functional group resins from various manufacturers are presented in *Table 2*, while the capacities determined for iminodiacetate functional group resins are shown in *Table 3*.

It was observed that the Al-binding capacity of aminomethylphosphonic resins significantly exceeded that of iminodiacetic resins – by nearly a factor of two – and showed a pronounced dependence on pH. Consequently, maintaining a stable and appropriate pH was found to be of critical importance both during experimental procedures and for potential industrial application. When the resin is in the H^+ form, acidification occurs during metal ion binding; conversely, when in the Na^+ form, alkalization takes place due to strongly basic hydrolysis reactions.

The results indicated that the capacity of aminomethylphosphonic acid resins reached a maximum within the pH range of 2.5 to 3. Furthermore, no significant difference in capacity was observed between the two manufacturers' products. In the case of iminodiacetic resins, the optimal pH appeared to be somewhat higher; however,

Table 2 | Total Al-binding capacity of aminomethylphosphonic acid resins at different pHs (mol Al / 1 L wet resin in Na^+ form)

pH	European manufacturer	Asian manufacturer
1.0	0.67 mol/L	0.67 mol/L
2.0	0.53 mol/L	0.56 mol/L
2.5	0.65 mol/L	0.71 mol/L
3.0	0.66 mol/L	0.70 mol/L
3.5	0.65 mol/L	0.66 mol/L
Without buffer	0.26 mol/L	0.26 mol/L
9.0	0.10 mol/L	0.09 mol/L
10.0	0.05 mol/L	0.04 mol/L
11.0	0.02 mol/L	0.01 mol/L

Source: Own work

Table 3 | Total Al-binding capacity of iminodiacetic acid resins at different pHs (mol Al / 1 L wet resin in Na^+ form)

pH	European manufacturer	Asian manufacturer
2.5	0.28 mol/L	0.27 mol/L
3.5	0.40 mol/L	0.37 mol/L
9.0	0.005 mol/L	0.004 mol/L
11.0	0.02 mol/L	0.03 mol/L

Source: Own work

fewer experiments were conducted with these materials due to their lower binding capacity, which made them less promising for aluminum removal.

Based on the data presented in *Table 2* and *Table 3*, it was also concluded that efficient operation of a mixed-bed resin system for the simultaneous removal of alkaline earth metal ions and aluminum is not feasible. This is due to the substantial difference in optimal pH: the iminodiacetate resin currently used for alkaline earth metal removal performs best at pH 7–9, which is markedly different from the optimal pH identified for aluminum removal with any of the resins investigated. As a result, the use of a dedicated ion exchange column for aluminum removal was considered necessary, with careful pH adjustment required prior to treatment.

Static kinetic study of metal ion binding by ion exchange

Static batch-shaking experiments were conducted at the previously determined optimal pH of 3, using an initial aluminum concentration of 1 ppm in Model 1 brine and varying degrees of resin saturation. The resulting kinetic data for the aminomethylphosphonic resins are presented in *Figure 2*, while the corresponding results for iminodiacetate resins are shown in *Figure 3*.

According to *Figure 2*, the behavior of the aminomethylphosphonic acid functionalized resins was found to be similar, although the resin from the European supplier demonstrated slightly higher efficiency. It was also observed that up to approximately 2% saturation, the aluminum-binding affinity of both resins remained nearly constant. However, at 3% saturation, the binding rate decreased considerably. Furthermore, at 20% saturation, the target residual aluminum concentration of 0.05 ppm could no longer be achieved in 5 hours with either resin, and therefore no further experiments were carried out beyond this point. Nonetheless, even a 2% utilization rate would represent an improvement over current industrial practice.

In the case of the two iminodiacetate functional group resins, *Figure 3* shows that their performance remained largely unchanged between 0% and 1% capacity utilization. However, at 2.5% saturation, aluminum binding

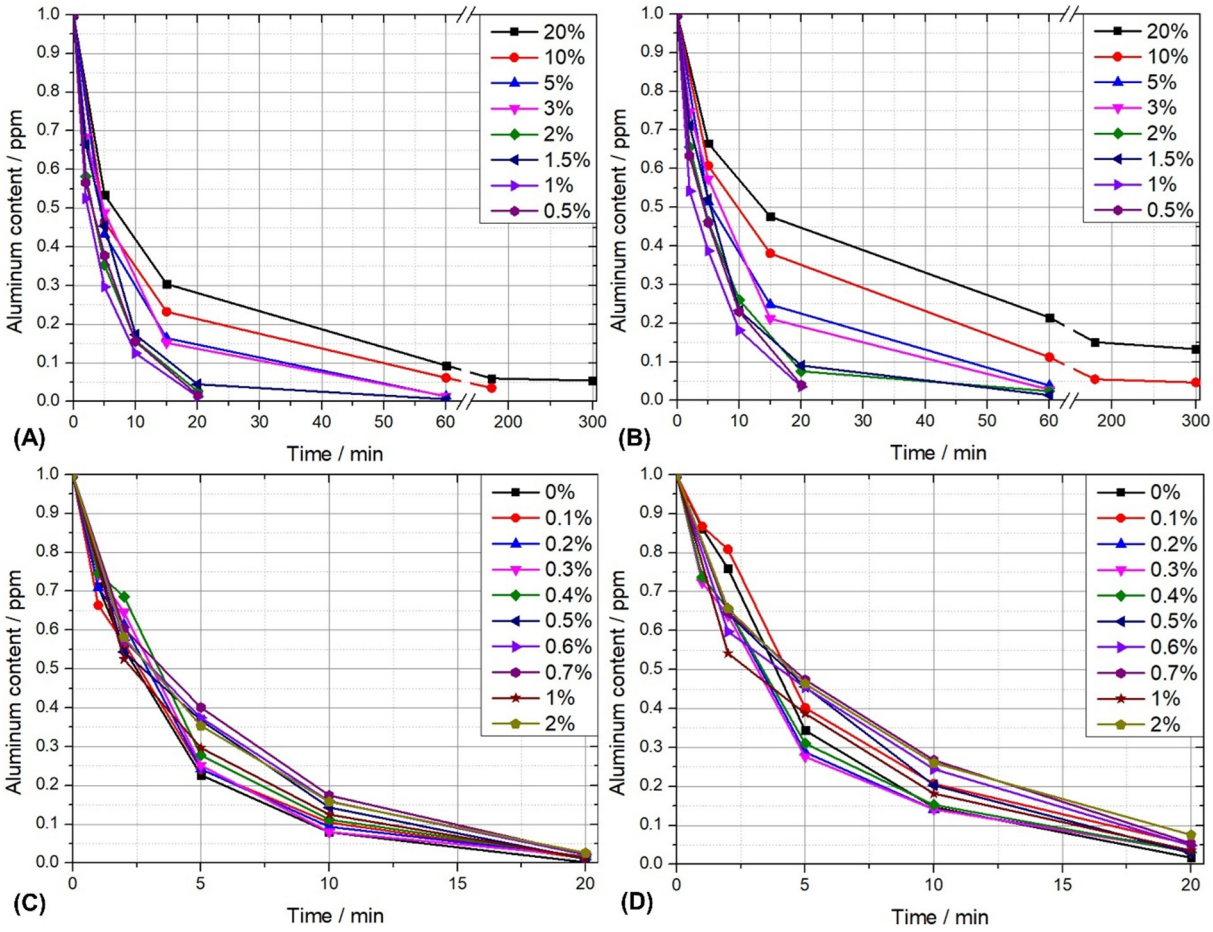

Figure 2 Investigation of the aluminum-binding affinity of aminomethylphosphonic resins from a European (left: A, C) and an Asian (right: B, D) manufacturer as a function of time and resin saturation. (The legend indicates the degree of saturation at the time of dosing the Al stock solution; complete binding under the experimental conditions corresponded to approximately a 0.1% increase in saturation.)

Source: Own work

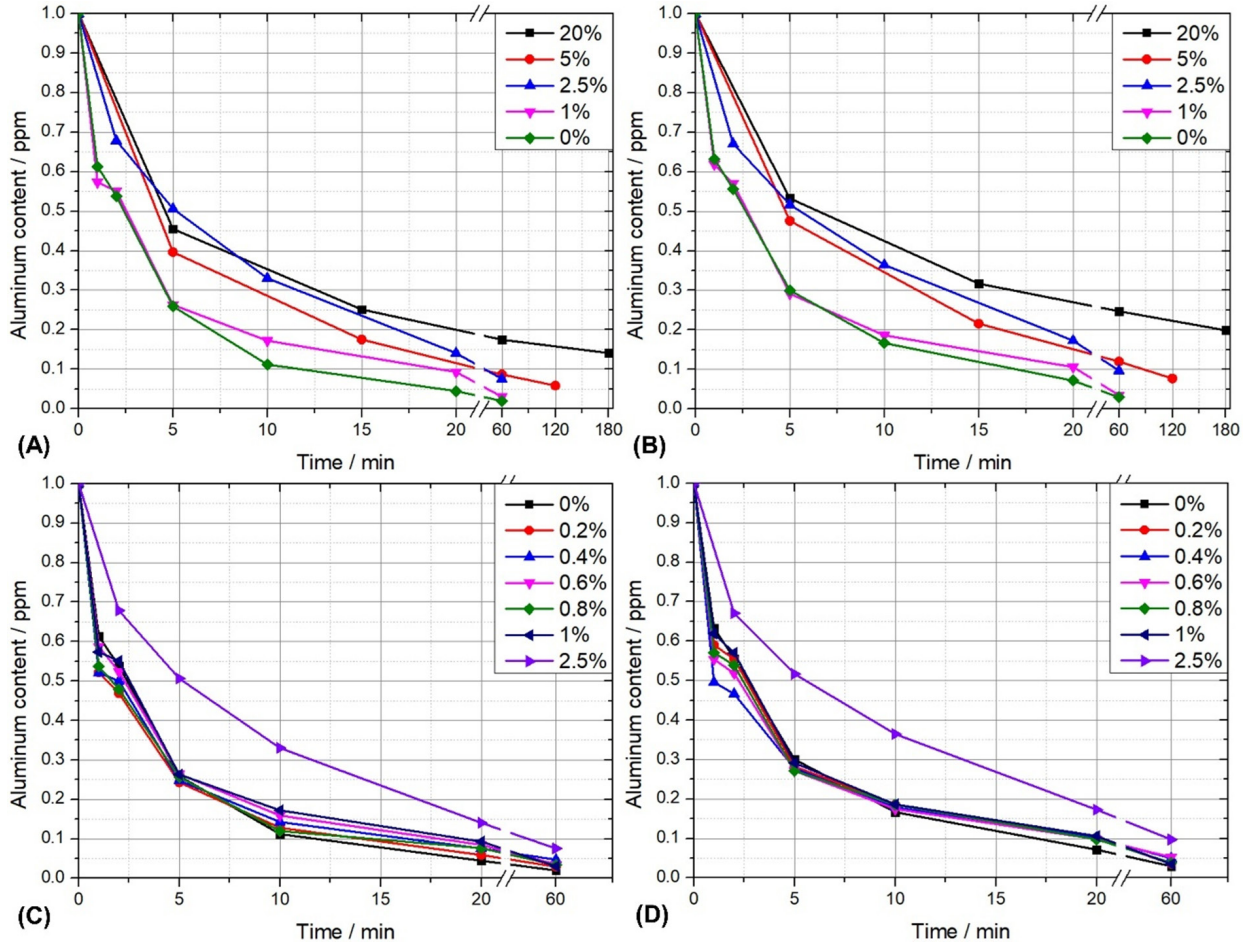

Figure 3 Investigation of the aluminum-binding affinity of iminodiacetate resins from a European (left: A, C) and an Asian (right: B, D) manufacturer as a function of time and resin saturation. (The legend indicates the degree of saturation at the time of dosing the Al stock solution; complete binding under the experimental conditions corresponded to approximately a 0.2% increase in saturation.)

Source: Own work

became significantly slower. As the residual aluminum content was already approximately 0.1 ppm after 20 minutes at only 1% saturation, the use of these resins beyond this point is not recommended.

It can therefore be concluded that, from the perspective of aluminum binding kinetics, the aminomethylphosphonic acid resins exhibit superior performance. Given that both their total aluminum-binding capacity (see *Table 2* and *Table 3*) and their effectively utilizable fraction are higher, these resins offer a significant advantage for aluminum removal. For these resins, reaction rate constants and liquid-side overall mass transfer coefficients were also determined, as described in the Appendix. Curve fitting results are also provided in the Appendix. Based on these fittings, it was confirmed that the pseudo-first-order kinetic model accurately describes the experimental data, with correlation coefficients (R^2) near 0.99 in all cases.

The liquid-side overall mass transfer coefficients calculated using the reaction rate constants obtained from curve fitting are presented in *Table 4*. It should be noted that in some cases, and within certain simulation software (e.g., Aspen), the applied β_F value may incorporate the specific surface area, a (in this context, defined relative to the total volume of the system in batch experiments, and thus differing from the value given in *Table 1*), or even the resin volume ratio ($1-\varepsilon_{out}$), i.e., the ratio of resin volume to total volume. For this reason, the values of $a \cdot \beta_L$ and $(a \cdot \beta_L)/(1-\varepsilon_{out})$ are also provided.

It is important to emphasize that the β_F values reported here can be considered more or less constant (although they may still be influenced by mixing conditions). However, the values of $a \cdot \beta_L$ and $(a \cdot \beta_L)/(1-\varepsilon_{out})$ are dependent on specific experimental or operational setups. In the simulations, it was assumed that the β_L values obtained under intensive shaking conditions adequately approximate the liquid-side overall mass transfer coefficients within the resin bed.

The data show that the overall mass transfer coefficient for the resin from the European supplier is higher than that of the resin from the Asian manufacturer. This indicates a kinetic advantage of the European resin, corroborating the conclusions drawn from *Figure 2*. This difference cannot be attributed to total binding capacity,

Table 4 Mass transfer coefficients determined for the different aminomethylphosphonic ion exchange resins

	European manufacturer		Asian manufacturer	
	20 °C	60 °C	20 °C	60 °C
k / s^{-1}	$4.99 \cdot 10^{-3}$	$9.96 \cdot 10^{-3}$	$3.09 \cdot 10^{-3}$	$7.91 \cdot 10^{-3}$
β_L/ ms^{-1}	$3.85 \cdot 10^{-9}$	$7.92 \cdot 10^{-9}$	$2.66 \cdot 10^{-9}$	$7.29 \cdot 10^{-9}$
$a \cdot \beta_L$/ s^{-1}	$3.13 \cdot 10^{-3}$	$6.67 \cdot 10^{-3}$	$1.95 \cdot 10^{-3}$	$5.50 \cdot 10^{-3}$
$\frac{a \cdot \beta_L}{1-\varepsilon_{out}}$ / s^{-1}	0.0976	0.201	0.0602	0.165

Source: Own work

as the resin from the Asian supplier has slightly higher capacity. The more favorable kinetic behavior may instead be explained by the more uniform, monodisperse particle size distribution of the European resin – consistent with the manufacturer's claims. The uniformity coefficient of this resin was below 1.1, a finding supported by our scanning electron microscopy-based particle size measurements. Specifically, the standard deviation of 20 particle diameters was found to be 0.018 mm for the European resin, compared to 0.12 mm for the Asian resin.

Similar kinetic experiments were also conducted for magnesium. The Mg-binding affinity of the unsaturated resins was examined in a manner analogous to the procedure used for aluminum, but at various pH values. The results are presented in *Figure 4*.

Based on the data in *Figure 4*, it can be concluded that neutral to mildly alkaline pH conditions are favorable for magnesium binding in the case of both iminodiacetate resins. Acidic conditions below pH 6 should be particularly avoided, as under such circumstances, neither resin was able to reduce the Mg content of the contacting solution below 0.25 ppm within 3 hours. The optimum pH was found to be pH 8 for the resin from the Asian manufacturer and pH 7 for the resin from the European manufacturer. At pH values above the optimum, only a slight decrease in binding efficiency was observed for both resins.

The figures also indicate that, under optimal pH conditions, a contact time of 5–10 minutes is sufficient to reduce the Mg concentration from 1 ppm to below 0.05 ppm.

This measurement further confirms that a dedicated ion exchange column is required for aluminum removal. Due to the significantly higher concentration of alkaline earth metal ions in brine, the use of the iminodiacetate resin is recommended as the first step in the purification process, followed by the aluminum removal column. This configuration is also favorable in terms of chemical consumption for pH adjustment. The unit operation preceding ion exchange is the sedimentation (and filtration) unit, where our previous studies *(Csorba et al. 2025)* have shown the optimal pH to be around 11. The process following ion exchange is the electrolyzer cell, where an acidic pH of approximately 2 is preferred to minimize the solubility of chlorine gas generated in the solution.

Accordingly, if the iminodiacetate-functionalized resin is used immediately after sedimentation, followed by the aminomethylphosphonic acid-functionalized resin, the initially alkaline pH can be gradually decreased in multiple steps. This is significantly more advantageous from the perspective of chemical consumption than if the order of the ion exchange columns were reversed, which would require adjusting the pH from 11 to 3, then to 7–8, and finally to 2.

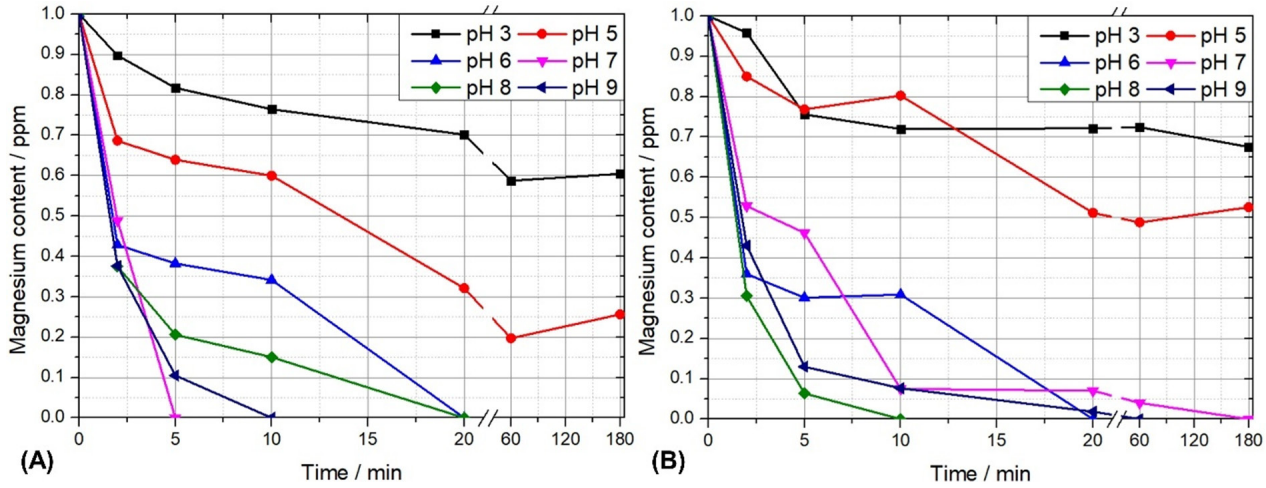

Figure 4 Evaluation of the Mg-binding affinity of iminodiacetate-functionalized resins from a European (left: A) and an Asian (right: B) manufacturer using initially unsaturated resins at an initial Mg concentration of 1 ppm. Under the given experimental conditions, the complete binding of 1 ppm Mg corresponds to approximately 0.3% of the total capacity of the resin. A Mg concentration marked as "0" on the figure indicates values below the photometric detection limit, i.e., below 0.03 ppm

Source: Own work

Dynamic investigation of aluminum binding, breakthrough curves

The temperature dependence of Al-binding efficiency and the effect of column geometry were investigated for aminomethylphosphonic resins under continuous operation, using a feed solution with an Al concentration of 0.5 ppm. The results are presented in *Figure 5* and *Figure 6*. For the breakthrough curves, the following logistic function was fitted to the measurement data points *(Hu et al. 2022)*:

$$c = \frac{c_0}{1+e^{-K\cdot(S-S_{50})}},$$

where c is the instantaneous Al content in the outlet flow, c_0 is the Al content in the inlet flow, K is fitting constant, S is the instantaneous saturation ratio, and S_{50} is the saturation ratio associated with the outlet concentration of $c_0/2$ (determined by linear interpolation from neighbouring data points).

According to *Figure 5*, the efficiency of aluminum removal increases markedly with rising temperature for both the European and Asian aminomethylphosphonic acid-based resins. This is evident from the fact that at higher temperature, at given degree of resin saturation, the aluminum concentration in the effluent is lower, and a higher saturation level corresponds to a given concentration limit. In the figure, a concentration limit of 0.05 ppm was arbitrarily chosen; in practice, the applicable threshold depends on the operating load of the electrolysis plant, and varies between 0.01 and 0.1 ppm.

The data also indicate that the ion exchange resin from the European manufacturer, which has a more uniform particle size distribution, performs more favorably than the reference product from the Asian supplier. For instance, at 60 °C, up to 50% of the resin capacity can be utilized before the effluent aluminum concentration reaches 0.05 ppm, compared to only 25% in the case of the Asian resin. Nevertheless, this latter value still exceeds the current capacity utilization of several electrolysis plants.

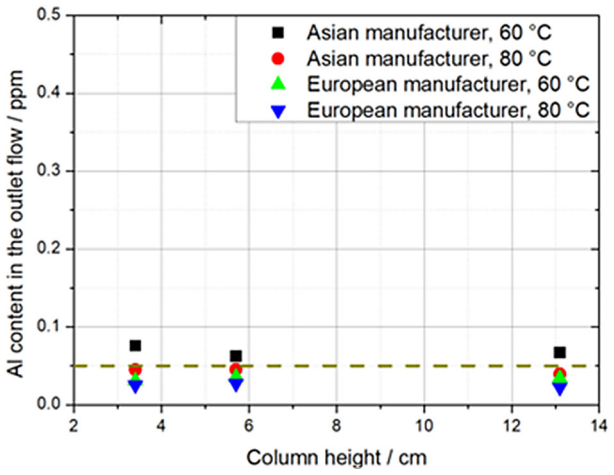

Figure 6 Effect of column geometry on the aluminum binding performance of aminomethylphosphonic ion exchange resins at 40% resin saturation

Source: Own work

Increasing resin utilization would result in less frequent regeneration cycles, thereby reducing water, chemical, and energy consumption, leading to operational cost savings and delivering important environmental benefits in terms of resource conservation.

Under full-capacity operation of the electrolysis unit, the performance gap between the two resins becomes even more pronounced. The European resin allows for 25% and 30% capacity utilization at an Al concentration

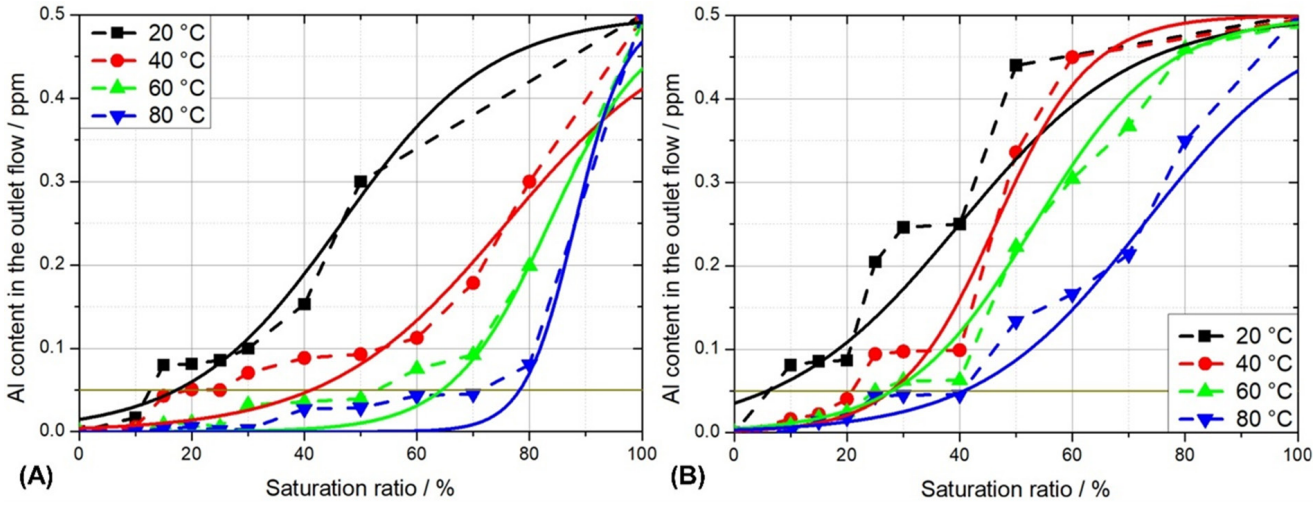

Figure 5 Effect of temperature and degree of saturation on the Al-binding capacity of aminomethylphosphonic ion exchange resins, left (A) for the European producer and right (B) for the Asian producer. The dashed line is used only to guide the eye, while the solid line indicates the fit according to the logistic function

Source: Own work

threshold of 0.01 ppm when operated at 60 °C and 80 °C, respectively. In contrast, the Asian reference resin only allows 5–10% utilization under the same conditions. Operation at or below 40 °C should be strongly avoided for both resins. As shown in *Figure 5*, the logistic function does not describe the results well in some cases, suggesting that there may be a discrepancy between the binding sites, for example due to space inhibition.

According to *Figure 6*, the geometry of the ion exchange column has no significant effect on the operational efficiency of aminomethylphosphonic acid-functionalized resins. Therefore, column design can be optimized based on other criteria, such as available space, cost, or pumpability.

At a 40% resin saturation level and 60 °C, the effect of additional metal contaminants on the aluminum binding efficiency was also investigated. The results indicate that when the feed brine contained 0.5 ppm Al along with 300 ppm Ca and 5 ppm Mg, no decrease in aluminum binding efficiency was observed. The same result was obtained when 1.5 ppm Fe was also present in the feed. This phenomenon may be related to the general valence selectivity of ion exchange processes, which typically favor ions with higher charge states *(Cséfalvay et al. 2012)*. However, it should be noted that the resin exhibited discoloration (browning) due to Fe-containing deposits. Based on previous operational experience, such iron-based coatings may gradually accumulate over months or years, forming a layer that cannot be removed by regeneration, ultimately considering the resin ineffective. In this regard, both the Asian reference resin and the European resin with identical functional groups showed similar behavior.

The adsorption isotherm describing aluminum binding onto aminomethylphosphonic acid resins was also determined, along with its parameters. Fitting the experimental equilibrium data to the Redlich–Peterson isotherm model did not converge reliably. Consequently, the constant b in the isotherm equation was fixed at a value of 1, yielding the Langmuir isotherm (in the publication Ma et al. *(2019)*, on which our simulation is based, $b = 0.97$ was optimal). In this case, the fit converged successfully, and the coefficient of determination (R^2) ranged between 0.93 and 0.98 across different conditions.

The average values of the K'/K ratio obtained from fitting at various temperatures (20 °C, 40 °C, 60 °C, 80 °C) were 0.979 mol/kg for the European resin and 0.943 mol/kg for the Asian resin. These values are in good agreement with the measured capacities of the resins, which were 0.94 mol/kg and 0.99 mol/kg, respectively.

Fitting was also performed using the Langmuir equation in the form *(Cséfalvay et al. 2012: 825)*:

$$q = \frac{q_{\max} \cdot K \cdot c}{1 + K \cdot c}.$$

The results for room temperature and the operationally relevant 60 °C are provided in the Appendix.

Considering that Al^{3+} ions are trivalent and may occupy three binding sites (based on charge balance: one Al^{3+} ion displaces three previously bound Na^+ or H^+ ions), an additional fit was performed using a modified Langmuir equation *(Cséfalvay et al. 2012: 827)*:

$$q = \frac{q_{\max} \cdot \sqrt[3]{K \cdot c}}{1 + \sqrt[3]{K \cdot c}}.$$

However, the R^2 values obtained from this model were significantly lower than those for the standard Langmuir model. Therefore, this approach was rejected. These findings suggest that the chelating aminomethylphosphonic acid functional group can bind Al^{3+} ions in a 1:1 molar ratio, and although three monovalent ions are released in the process, the functional group should be considered a single binding site with respect to Al^{3+}.

As expected, favorable isotherm curves were obtained in all cases. In line with experimental observations, the equilibrium constant K for the European resin was significantly higher (2–3 times) than that of the competing Asian resin at both examined temperatures (shown in *Table 5*). Furthermore, a clear positive effect of temperature was observed: the equilibrium constant increased substantially (by a factor of 3–5) between 20 °C and 60 °C. This confirms that the binding reaction (involving desorption of initially bound H^+ or Na^+ ions) is endothermic.

In addition to the equilibrium constant, the selectivity factor (T) and the distribution coefficient (d) were also calculated and are presented in *Table 5*. Although these parameters are associated with relatively high uncertainty, the same trends observed for the equilibrium constant were confirmed: the resin from the European manufacturer performed more efficiently, and increased temperature facilitated the binding reaction.

Table 5 Equilibrium constants, selectivity coefficients, and distribution ratios for aluminum binding on aminomethylphosphonic ion exchange resins

	European manufacturer		Asian manufacturer	
	20 °C	60 °C	20 °C	60 °C
K	$8.9 \cdot 10^4$	$4.7 \cdot 10^5$	$4.7 \cdot 10^4$	$1.6 \cdot 10^5$
T	$1.6 \cdot 10^5$	$9.7 \cdot 10^5$	$7.9 \cdot 10^4$	$3.1 \cdot 10^5$
d	$9.5 \cdot 10^4$	$4.6 \cdot 10^5$	$5.1 \cdot 10^4$	$1.9 \cdot 10^5$

Source: Own work

Detailed simulation of ion exchange based on the Homogeneous Surface Diffusion Model (HSDM) using the Crank-Nicolson algorithm

Basis of the simulation program

The simulation program was developed based on the Homogeneous Surface Diffusion Model (HSDM), following the methodology of Ma et al. *(2019)* (for details, see the Introduction section). The model was subsequently validated using literature data *(Ma et al 2019)*, implemented using our own experimental data, with initial simulations conducted under laboratory conditions at 60 °C, using data obtained from both the European and the Asian manufacturers' aminomethylphosphonic acid-functionalized ion exchange resins. For the simulations, parameters corresponding to 60 °C – such as Langmuir constants and mass transfer coefficients – were applied. The results are presented in *Figure 7*.

Based on *Figure 7*, it can be concluded that the simulation results are consistent with the experimental data, as breakthrough occurs within the expected time range. If the ion exchange resin were capable of binding the entire 0.5 ppm inlet Al content, full saturation would occur after approximately 1,000 hours, or 42 days. According to the measurements, the resin from the European manufacturer allows for 70% capacity utilization under uniform saturation and a 0.1 ppm outlet concentration limit, while the resin from the Asian manufacturer allows for 40%, which corresponds to 20–30 days of operation. According to the simulation, breakthrough occurs between days 28 and 32, which is in agreement with the anticipated range.

It is important to note that in the experiments, the ion exchange resin was statically pre-saturated to various fractions of full capacity, and this partially loaded resin was then used in the dynamic experiments. Therefore, the Al concentration profile in the resin within the resin bed along the column length can be approximated as a near-constant function. Compared to the isochrones shown in *Figure 7*, this may lead to slightly earlier breakthrough, as the rear section of the resin bed is already in a more saturated state. Conversely, if the rear section were in a less saturated state (compensated by a more heavily loaded front section), it could still bind aluminum ions that pass through the initial zone.

Additionally, the breakthrough may appear delayed relative to the 20–30 day estimate because that estimate assumes 100% binding efficiency until breakthrough. In reality, efficiency begins to decline (to 80–90%) prior to breakthrough, meaning only 80–90% of the incoming aluminum is retained by the resin, resulting in slower overall saturation. This confirms that the results obtained through simulation are realistic.

Figure 7 also illustrates how the resin bed gradually becomes saturated during dynamic operation, and how the internal concentration profile propagates through the resin bed over time. The effect of resin bed length can also be inferred from the figure: if the resin bed were shortened – for example, to 4 cm – breakthrough would occur earlier, around 3 weeks (slightly later for the European resin, slightly earlier for the Asian one).

The simulation also confirms the superior performance of the European resin: at a given position, the isoplanes show that the same concentration is reached later compared to the Asian resin (the isoplanes for the Asian resin are shifted forward), and at a given time, the isochrones indicate lower concentrations for the European resin (its isochrones lag behind those of the Asian resin).

Following this, upscaling to industrial dimensions was simulated. Keeping the relative flow rate constant at 30

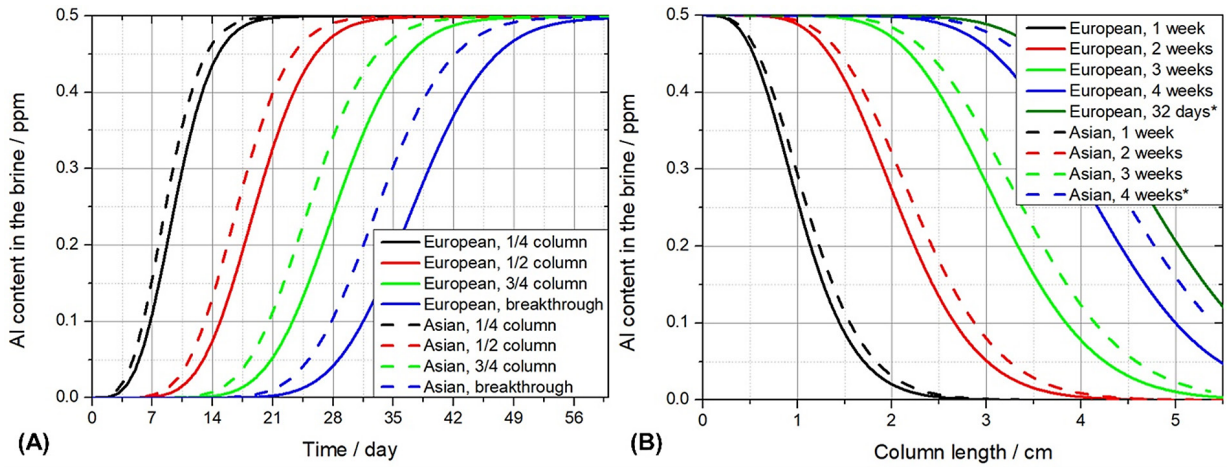

Figure 7 Results of the simulation based on the HSDM, carried out using data from dynamic laboratory experiments performed at 60 °C with an inlet Al concentration of 0.5 ppm: isoplanes (left: A) and isochrones (right: B). The breakthrough point – defined as the time when the outlet Al concentration exceeds the threshold of 0.1 ppm – is marked with an asterisk (*)

Source: Own work

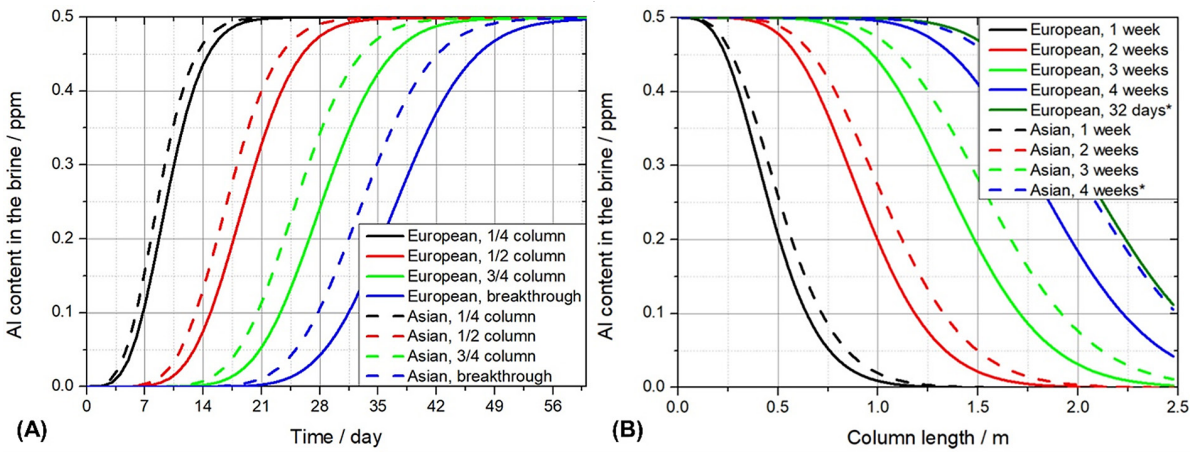

Figure 8 Results of the simulation based on the HSDM for industrial-scale ion exchange at 60 °C and with an inlet Al concentration of 0.5 ppm: isoplanes (left: A) and isochrones (right: B). The breakthrough point – defined as the time when the outlet Al concentration exceeds the threshold of 0.1 ppm – is marked with an asterisk (*)

Source: Own work

BV/h, with an inlet Al concentration of 0.5 ppm and a temperature of 60 °C, the resin bed was expanded to a size representative of industrial practice – approximately 2.5 m in diameter and height – with the absolute flow rate adjusted accordingly. The results of the scaled-up simulation are shown in *Figure 8*.

Figure 7 and *Figure 8* show a high degree of similarity; neither the isoplanes nor the isochrones changed significantly as a result of the scale-up, nor did the breakthrough time. Based on this, it can be concluded that, according to the simulation, scaling up to industrial dimensions is feasible.

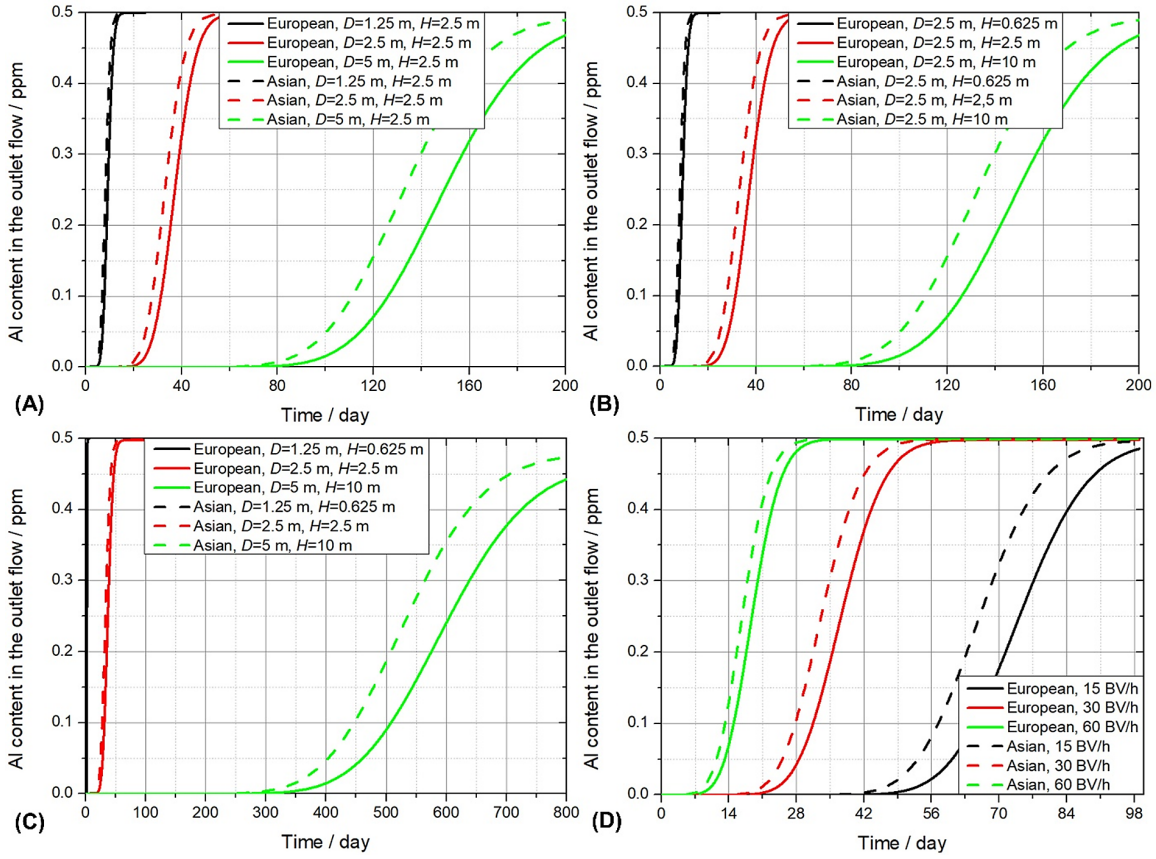

Figure 9 Simulation results based on the HSDM under industrial-scale ion exchange conditions at 60 °C and an inlet Al concentration of 0.5 ppm: the effect of resin volume and resin bed column geometry on breakthrough curves at a brine flow rate of 30 BV/h (A, B, C), and the effect of the relative brine flow rate (D)

Source: Own work

Sensitivity analyses

Using the simulation under industrial conditions, several sensitivity analyses were also performed. An investigation of resin particle size indicated that smaller particles enable slightly more efficient removal. However, the difference identified in the simulation was not significant. It should be noted, though, that this result was obtained while keeping all other parameters (such as mass transfer coefficients and Langmuir constants) unchanged, whereas in reality, particle size may also affect these parameters. Therefore, a greater impact on removal efficiency could be expected indirectly.

The effect of column geometry was also found to be negligible, which confirms the experimental results. However, the relative flow rate (with respect to resin volume), the quantity of resin, and the inlet aluminum concentration of the brine had a significant effect on the breakthrough curves, isochrones and isoplanes, and thus on the overall removal efficiency. The results of these sensitivity analyses are shown in *Figure 9* and *Figure 10*.

According to *Figure 9*, keeping all other parameters constant, as the flow rate increases, breakthrough occurs earlier. This is unsurprising, as a higher brine flow leads to faster saturation of the ion exchange resin. Nevertheless, it can be concluded that even at a flow rate of 60 BV/h, the resin is still capable of adequately purifying the brine until saturation, indicating that sufficient residence time is available to ensure binding.

For the resin from the European manufacturer, breakthrough occurs on day 65 at 15 BV/h, on day 32 at 30 BV/h, and at the very beginning of day 16 at 60 BV/h. For the resin from the Asian manufacturer, these values are day 58, day 28, and day 14, respectively.

Figure 9 also shows that there is a linear relationship between the amount (volume) of resin and the breakthrough time, if all other parameters are kept constant. This is in line with expectations. It is also apparent that the effect of increasing resin volume is practically the same whether the cross-sectional area of the column is increased by doubling the diameter (thus quadrupling the area) or the height is increased fourfold. This is clearly visible in the top two graphs of *Figure 9*, which show nearly identical breakthrough curves in both cases. Similar results were obtained when the resin volume was reduced by either method. This outcome is also consistent with the earlier findings concerning the effect of column geometry.

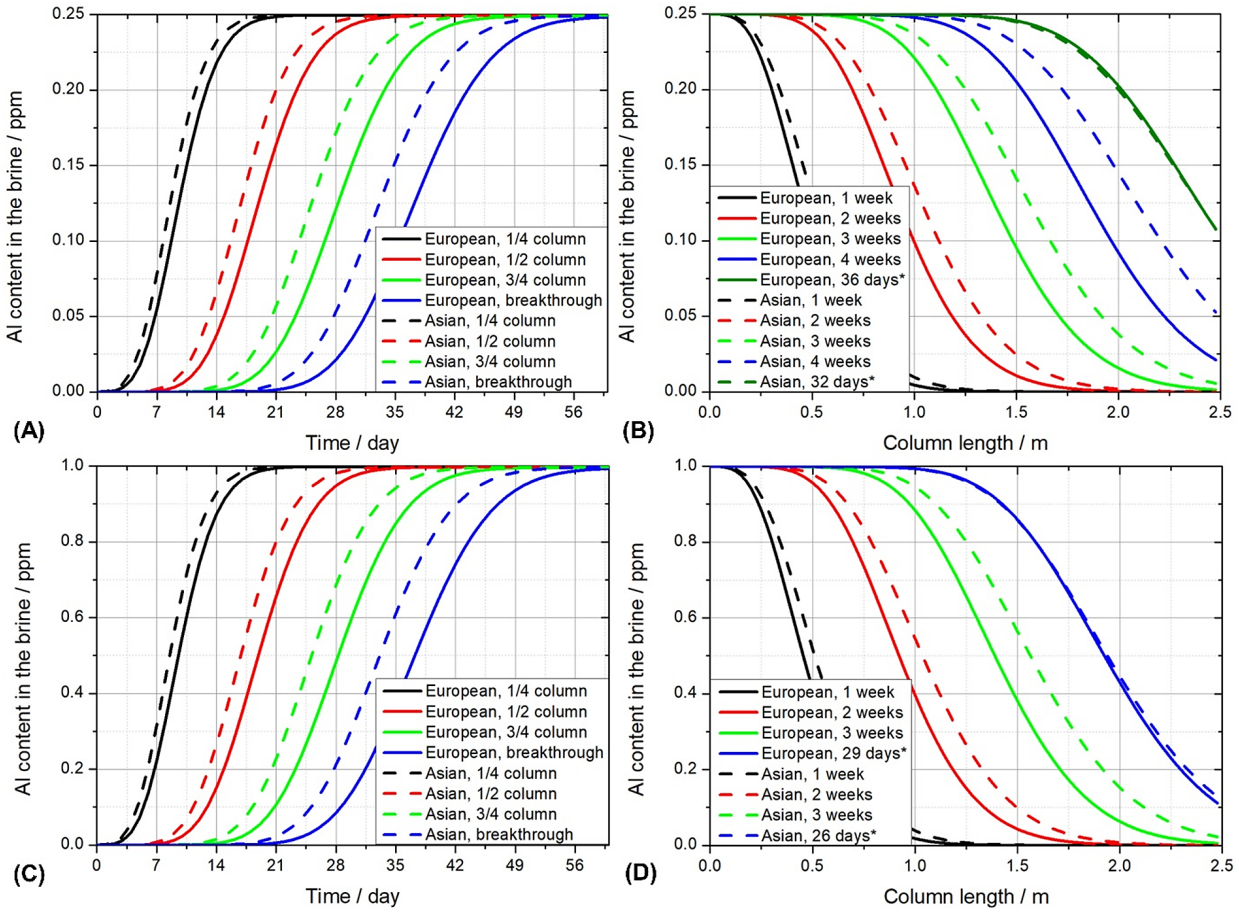

Figure 10 Simulation results based on the HSDM under industrial-scale ion exchange conditions at 60 °C: the effect of inlet brine Al concentration on isoplanes (A, C) and isochrones (B, D) at inlet Al concentrations of 0.25 ppm (A, B) and 1 ppm (C, D)

Source: Own work

According to *Figure 10* (and, for comparison, *Figure 8*, which was generated using the original inlet Al concentration of 0.5 ppm), the results concerning the effect of inlet Al concentration align with the initial expectations: higher inlet concentrations lead to earlier saturation and, consequently, earlier breakthrough. However, upon doubling the inlet Al concentration, breakthrough did not occur in half the time, but considerably later. For the resin from the European manufacturer, breakthrough occurred on day 36 at an inlet concentration of 0.25 ppm, on day 32 at 0.5 ppm, and on day 29 at 1.0 ppm. For the resin from the Asian manufacturer, these values were day 32, day 28, and day 26, respectively.

This phenomenon may be attributed to kinetic factors. At higher inlet Al concentrations, the driving force for mass transfer increases – the difference between the instantaneous Al concentration in the liquid phase and the equilibrium concentration corresponding to the actual saturation state of the resin. Accordingly, with a higher inlet Al concentration, the aluminum content in the solution decreases more steeply along the initial section of the column. For instance, at 1.0 ppm inlet concentration, after one week of operation, the Al concentration of 0.5 ppm (corresponding to the reference case) is already reached at a column height of around 0.5 meters (slightly earlier for the European resin and slightly later for the Asian resin). Thus, this concentration level is achieved within the first fifth of the column, leaving the remaining four-fifths available for further reduction of the Al content below 0.5 ppm.

This result is highly favorable from an operational perspective: a temporary increase in inlet Al concentration is not expected to cause significantly earlier breakthrough. Therefore, even if the resin bed is exposed to brine with elevated Al concentrations for a limited period, the duration of an individual operational cycle will not be substantially reduced.

Conclusion

In the chlor-alkali industry, the most modern, environmentally friendly, and energy-efficient technology is the membrane cell method. However, this process requires significantly purer brine compared to previous technologies. The removal of alkaline earth metals was already well established, but further improvements were needed for aluminum.

Ion exchange methods for the removal of residual Al^{3+} ions after the precipitation, sedimentation and filtration process were investigated. Several ion exchange resins were characterized. Aminomethylphosphonic resins are effective for Al removal, the optimal pH interval is 2.5–3.0. This is substantially different from the weakly alkaline pH optimal for alkaline earth metal binding using iminodiacetic resins, necessitating a separate ion exchange column against aluminum. Simultaneous removal using mixed resin bed is therefore not feasible. Among the examined resins from various manufacturers, capacity utilization above 50% is achievable while keeping the 0.1 ppm Al content limit needed for membrane technology. This extended cycle time reduces the fluctuations of aluminum concentration (since the column spends less time in regeneration phase) and leads to cost savings by lowering chemical consumption,

Furthermore, simulations of the brine purification process were also conducted. The ion exchange process was simulated in detail using a self-made program based on the homogeneous surface diffusion model (HSDM), examining the effects of flow rate, brine composition, bed geometry and resin quantity, including industrial scaling. The resulting breakthrough curves, isoplanes, and isochrones were consistent with our experimental results. Based on the simulation, the ion exchange system can also effectively handle fluctuations in the aluminum content of the inlet brine as well as in the volume flow rate.

Based on our work, BorsodChem Ltd. has installed one additional ion exchange column containing aminomethylphosphonic acid functionalized resin – *dedicated specifically for aluminum removal* – in both membrane cell units. These columns are filled with 13 m^3 of resin, and the brine solution at 60 °C flows continuously through them at a rate of 30 BV/h. According to operational experience, the column has proven to be effective in removing aluminum to levels *in accordance with BAT limits*, contributing to the *safe operation* of the technology.

Acknowledgements

Project no. C1340882 has been implemented with the support provided by the Ministry of Culture and Innovation of Hungary from the National Research, Development and Innovation Fund, financed under the KDP-2021 funding scheme.

The support of the project by Wanhua-BorsodChem Ltd., Kazincbarcika, Hungary, is greatly appreciated. B. Csorba, P. Tóth, A. Mihalkó, L. Farkas, and R. Z. Boros thank the support of Tamás Purzsa, Senior Chief Advisor, and Zhao Nan Deputy Chief General Engineer. The authors thank Aranka Máté and Zsolt Martinkó for their help and for conducting laboratory experiments as well.

References

Anthoni, J. F. (2006) The chemical composition of seawater. Magnesium, Vol. 2701. No. 96. p. 9062.

Binega, Y. (2006) Chemical analysis of the assale (Ethiopia) rock salt deposit. Bulletin of the Chemical Society of Ethiopia, Vol. 20. No. 2. pp. 319–324. https://doi.org/10.4314/bcse.v20i2.21174

Blokhin, A. A., Murashkin, Y. V., & Mikhaylenko, M. A. (2021) Iron (III) removal from aluminum sulfate solutions by sorption. Russian Journal of Applied Chemistry, Vol. 94. No. 6. pp. 813–817. https://doi.org/10.1134/S1070427221060148

Brée, L. C., Bulan, A., Herding, R., Kuhlmann, J., Mitsos, A., Perrey, K., & Roh, K. (2020) Techno-economic comparison of flexibility options in chlorine production. Industrial & Engineering Chemistry Research, Vol. 59. No. 26. pp. 12186–12196. https://doi.org/10.1021/acs.iecr.0c01775

Chen, C.-C., Britt, H. I., Boston, J. F., & Evans, L. B. (1982) Local composition model for excess Gibbs energy of electrolyte systems. Part I: Single solvent, single completely dissociated electrolyte systems. AIChE Journal, Vol. 28. No. 4. pp. 588–596. https://doi.org/10.1002/aic.690280410

Chen, C.-C. & Evans, L. B. (1986) A local composition model for the excess Gibbs energy of aqueous electrolyte systems. AIChE Journal, Vol. 32. No. 3. pp. 444–454. https://doi.org/10.1002/aic.690320311

Chidambaran, R., Bisht, N. S., & Raina, P. (2014) Water treatment process. World Intellectual Property Organization International Bureau, Patent No. WO 2014/088,826 A1.

Çiçek, A., Yilmaz, O., & Arar, O. (2018) Removal of lithium from water by aminomethylphosphonic acid containing resin. Environmental Chemistry, Vol. 83. No. 9. pp. 1059–1069. https://doi.org/10.2298/JSC170930020C

Costa, H. P. S., Silva, M. G. C., & Vieira, M. G. A. (2021) Fixed bed biosorption and ionic exchange of aluminum by brown algae residual biomass. Journal of Water Process Engineering, Vol. 42. e102117. https://doi.org/10.1016/j.jwpe.2021.102117

Cséfalvay E., Deák A., Farkas T., Hanák L., Mika L. T., Mizsey P., … Vágó E. (2012) Vegyipari műveletek II. Anyagátadó műveletek és kémiai reaktorok. (ed. Simándi B.) Budapest, Typotex Kiadó. https://oszkdk.oszk.hu/storage/00/00/59/33/dd/1/simandi_animaciok_nelkul.pdf [Accessed: 28/01/2025].

Csorba B., Farkas L., Csécsi M., Hórvölgyi Z., Szabó T., Madarász J., … Gresits I. L. (2025) Removal of aluminum content of concentrated salt solutions by precipitation, coagulation and sedimentation. Chemical Papers, Vol. 79. pp. 4109–4130. https://doi.org/10.1007/s11696-025-03942-8

Csorba B., Farkas L., Csécsi M., Mika L. T., & Gresits I. L. (2024) Facile determination of aluminum content in industrial brine by investigating the effects of buffer systems. ChemistryOpen, Vol. 13. No. 12. e202400038. https://doi.org/10.1002/open.202400038

Csorba B., Farkas L., Mihalkó A., Boros R. Zs., & Gresits I. L. (2023) Photometric determination of trace amounts of aluminum in nearly saturated rock salt solutions used by chlor-alkali industry. Periodica Polytechnica Chemical Engineering, Vol. 67. No. 3. pp. 442–451. https://doi.org/10.3311/PPch.22051

Das, J. & Pobi, M. (1991) Separation of beryllium and aluminum from other elements using an ion-exchange resin with IV-benzoylphenylhydroxylamine as a functional group. Analytica Chimica Acta, Vol. 242. pp. 107–111. https://doi.org/10.1016/0003-2670(91)87053-A

Ding, J., Hua, W., Zhang, H., & Lou, Y. (2013) The development and application of two chlorine recycling technologies in polyurethane industry. Journal of Cleaner Production, Vol. 41. pp. 97–104. https://doi.org/10.1016/j.jclepro.2012.09.020

European Commission (2014) JRC Publications repository – Best Available Techniques (BAT) reference document for the production of chlor-alkali. Industrial Emissions Directive 2010/75/EU (Integrated Pollution Prevention and Control). https://publications.jrc.ec.europa.eu/repository/handle/JRC91156 [Accessed: 15/01/2025].

European Commission (2020) Scientific Committee on Consumer Safety (SCCS): Opinion on the safety of aluminum in cosmetic products – Submission II. https://health.ec.europa.eu/system/files/2021-11/sccs_o_235.pdf [Accessed: 15/05/2025].

Fauvarque, J. (1996) The chlorine industry. Pure and Applied Chemistry, Vol. 68. No. 9. pp. 1713–1720. https://doi.org/10.1351/pac199668091713

Feng, X., Li, P., Fu, X., Wang, X., Zhang, H., & Lin, C. J. (2022) Mercury pollution in China: implications on the implementation of the Minamata Convention. Environmental Science: Processes & Impacts, Vol. 24. No. 5. pp. 634–648. https://doi.org/10.1039/D2EM00039C

Fengmin, D., Warsinger, D. M., Urmi, T. I., Thiel, G. P., Kumar, A., & Lienhard V. J. H. (2018) Sodium hydroxide production from seawater desalination brine: Process design and energy efficiency. Environmental Science & Technology, Vol. 52. No. 10. pp. 5949–5958. https://doi.org/10.1021/acs.est.8b01195

Franco, P. E., Veit, M. T., Borba, C. E., da Cunha Gonçalves, G., Fagundes-Klen, M. R., Bergamasco, R., … Suzaki, R. Y. R. (2013) Nickel(II) and zinc(II) removal using Amberlite IR-120 resin: Ion exchange equilibrium and kinetics. Chemical Engineering Journal, Vol. 221. pp. 426–435. https://doi.org/10.1016/j.cej.2013.02.006

Gallindo, A. D. A. S., da Silva Junior, R. A., Rodrigues, M. G. F., & Ramos, W. B. (2021) Modelling and simulation of the ion exchange process for Zn^{2+} (aq) removal using zeolite NaY. Research, Society and Development, Vol. 10. No. 12. e310101220362. https://doi.org/10.33448/rsd-v10i12.20362

García, E., Rodriguez, L., Ferro, V., & Valverde, J. L. (2019) Prediction of multicomponent ION exchange equilibria by using the e-NRTL model for computing the activity coefficients in solution. Fluid Phase Equilibria, Vol. 498. pp. 132–143. https://doi.org/10.1016/j.fluid.2019.07.002

Hem, J. D. & Roberson, C. E. (1967) Form and stability of aluminum hydroxide complexes in dilute solution. Washington, United States Government Printing Office. https://pubs.usgs.gov/wsp/1827a/report.pdf [Accessed: 13/02/2025].

Hérés, X., Blet, V., Natale, P. D., Ouaattou, A., Mazouz, H., Dhiba, D., & Frederic, C. (2018) Selective extraction of rare earth elements from phosphoric acid by ion exchange resins. Metals, Vol. 8. No. 9. pp. 682. https://doi.org/10.3390/met8090682

Hermassi, M., Granados, M., Valderrama, C., Ayora, C., & Cortina, J. L. (2021) Recovery of rare earth elements from acidic mine waters by integration of a selective chelating ion-exchanger and a solvent impregnated resin. Journal of Environmental Chemical Engineering, Vol. 9. No. 5. e105906. https://doi.org/10.1016/j.jece.2021.105906

Horton, A. D. & Thomason, P. F. (1956) Ion exchange-spectrophotometric determination of aluminum. Analytical Chemistry, Vol. 28. No. 8. pp. 1326–1328. https://doi.org/10.1021/ac60116a031

Hossain, N., Bhattacharia, S. K., & Chen, C.-C. (2016) Temperature dependence of interaction parameters in electrolyte NRTL model. AIChE Journal, Vol. 62. No. 4. pp. 1244–1253. https://doi.org/10.1002/aic.15080

Hossain, N., Ravichandran, A., Khare, R., & Chen, C.-C. (2018) Revisiting Electrolyte Thermodynamic Models: Insights from Molecular Simulations. AIChE Journal, Vol. 64. No. 10. pp. 3728–3734. https://doi.org/10.1002/aic.16327

Hu, Q., Wang, D., Pang, S., & Xu, L. (2022) Prediction of breakthrough curves for multicomponent adsorption in a fixed-bed column using logistic and Gompertz functions. Arabian Journal of Chemistry, Vol. 15. No. 9. e104034. https://doi.org/10.1016/j.arabjc.2022.104034

Humphreys, J., Lan, R., & Tao, S. (2021) Development and recent progress on ammonia synthesis catalysts for Haber–Bosch process. Advanced Energy and Sustainability Research, Vol. 2. No. 1. e2000043. https://doi.org/10.1002/aesr.202000043

Hydes, D. J. (1979) Aluminum in seawater: Control by inorganic processes. Science, Vol. 205. No. 4412. pp. 1260–1262. https://doi.org/10.1126/science.205.4412.1260

Ingman, F. & Ringbom, A. (1966) Spectrophotometric determination of small amounts of magnesium and calcium employing Calmagite. Microchemical Journal, Vol. 10. No. 1–4. pp. 545–553. https://doi.org/10.1016/0026-265X(66)90239-6

Jie, G. & Yonggao, X. (2021a) Method for recovering iron phosphate from iron-phosphorus slag after lithium extraction of lithium iron phosphate lithium battery. Chinese Patent, No. CN 111,646,447 B.

Jie, G. & Yonggao, X. (2021b) Method for recovering lithium from waste lithium iron phosphate batteries and method for recovering lithium and iron phosphate. Chinese Patent, No. CN 111,675, 203 B.

Kiefer, R. & Höll, W. H. (2001) Sorption of heavy metals onto selective ion-exchange resins with aminophosphonate functional groups. Industrial & Engineering Chemistry Research, Vol. 40. No. 21. pp. 4570–4576. https://doi.org/10.1021/ie010182l

Kirkes, T. E., Saravi, S. H., & Chen, C.-C. (2021) Thermodynamic modeling of aqueous LiCl, LiBr, LiI, and $LiNO_3$ solutions. Fluid Phase Equilibria, Vol. 531. e112914. https://doi.org/10.1016/j.fluid.2020.112914

Kurkinen, S., Virolainen, S., & Sainio, T. (2021) Recovery of rare earth elements from phosphogypsum waste in resin-in-leach process by eluting with biodegradable complexing agents. Hydrometallurgy, Vol. 201. e105569. https://doi.org/10.1016/j.hydromet.2021.105569

LANXESS Deutschland GmbH (2024) LANXESS – Products & Brands – LEWATIT MonoPlus TP 208. https://Lanxess.com/en-us/products-and-brands/products/L/Lewatit--monoplus-tp-208 [Accessed: April 2, 2025].

Le Bihan, A., Lijour, Y., Giamarchi, P., Burel-Deschamps, L., & Stephan, L. (2003) Direct determination of aluminum content in seawater by electrothermal atomization-laser excited atomic fluorescence. Spectrochimica Acta Part B: Atomic Spectroscopy, Vol. 58. No. 1. pp. 15–26. https://doi.org/10.1016/S0584-8547(02)00200-8

Li, J., Koner, S., German, M., & SenGupta, A. K. (2016) Aluminum-cycle ion exchange process for hardness removal: A new approach for sustainable softening. Environmental Science & Technology, Vol. 50. No. 21. pp. 11943–11950. https://doi.org/10.1021/acs.est.6b03021

Liu, X., Ouyang, J., Zhang, C., Wang, Z., Zhou, Q., Chen, Z., … Liu, C. (2023) Comprehensive recycling method for waste lithium iron phosphate battery. US Patent, No. US 2023/0,050,044 A1.

Ma, A., Abushaikha, A., Allen, S. J., & McKay, G. (2019) Ion exchange homogeneous surface diffusion modelling by binary site resin for the removal of nickel ions from wastewater in fixed beds. Chemical Engineering Journal, Vol. 358. pp. 1–10. https://doi.org/10.1016/j.cej.2018.09.135

Marcin, M. A. & Sage, T. R. (2017) System and method for treatment of produced waters. US Patent, No. US 9,719,179 B2.

Margallo, M., Onandía, R., Aldaco, R., & Irabien, A. (2016) When life cycle thinking is necessary for decision making: Emerging cleaner technologies in the chlor-alkali industry. Chemical Engineering Transactions, Vol. 52. pp. 475–480. https://doi.org/10.3303/CET1652080

Mc Lein Roger, M., Manacup, C. V. L., Soriano, A. N., & Rubi, R. V. C. (2023) Continuous biosorption of Pb^{2+} with bamboo shoots (Bambusa spp.) using Aspen Adsorption Process Simulation Software. ASEAN Journal of Chemical Engineering, Vol. 23. No. 2. pp. 153–166. https://doi.org/10.22146/ajche.77314

Millero, F. J., Feistel, R., Wright, D. G., & McDougall, T. J. (2008) The composition of standard seawater and the definition of the Reference-Composition Salinity Scale. Deep Sea Research Part I: Oceanographic Research Papers, Vol. 55. No. 1. pp. 50–72. https://doi.org/10.1016/j.dsr.2007.10.001

Minamata Convention on Mercury (2021) Parties and Signatories. https://www.mercuryconvention.org/en/parties [Accessed: 2/02/2025].

Namana, S. B., Pullagurla, H. R., Nallamudi, J., Kumar, K. K., & Pitta, B. R. (2024) Preparation of high-purity manganese sulfate and removal of unwanted metal ions using resin-based purification. Canadian Metallurgical Quarterly, Vol. 64. No. 4. pp. 2313–2323. https://doi.org/10.1080/00084433.2024.2417498

Nye, P., Craig, D., Coleman, N. T., & Ragland, J. L. (1961) Ion exchange equilibria involving aluminum. Soil Science Society of America Journal, Vol. 25. No. 1. pp. 14–17. https://doi.org/10.2136/sssaj1961.03615995002500010012x

Ogunbiyi, O., Saththasivam, J., Al-Masri, D., Manawi, Y., Lawler, J., Zhang, X., & Liu, Z. (2021) Sustainable brine management from the perspectives of water, energy and mineral recovery: A comprehensive review. Desalination, Vol. 513. e115055. https://doi.org/10.1016/j.desal.2021.115055

Pátzay G., Tungler A., & Mika L. T. (2011) Kémiai technológia. Budapest, Typotex. https://oszkdk.oszk.hu/storage/00/00/59/39/dd/1/Kemiai_technologia_animacio_nelkul.pdf [Accessed: 28/01/2025].

Petrie, J. J. J. B., Fleming, R., McKinnon, P., Winney, R. J., & Cowie, J. (1984) The use of ion exchange to remove aluminum from water used in hemodialysis. American Journal of Kidney Diseases, Vol. 4. No. 1. pp. 69–74. https://doi.org/10.1016/S0272-6386(84)80030-X

Popat, K. M., Anand, P. S., & Dasare, B. D. (1994) Selective removal of fluoride ions from water by the aluminum form of the aminomethylphosphonic acid-type ion exchanger. Reactive Polymers, Vol. 23. No. 1. pp. 23–32. https://doi.org/10.1016/0923-1137(94)90107-4

Ramírez, Y., Cisternas, L. A., & Kraslawski, A. (2017) Application of house of quality in assessment of seawater pretreatment technologies. Journal of Cleaner Production, Vol. 148. pp. 223–232. https://doi.org/10.1016/j.jclepro.2017.01.163

Recepoglu, Y. K. (2024) Optimized Lithium(I) Recovery from geothermal brine of Germencik, Türkiye, utilizing an aminomethyl phosphonic acid chelating resin. Solvent Extraction and Ion Exchange, Vol. 43. No. 1. pp. 23–44. https://doi.org/10.1080/07366299.2024.2404146

Rubin, A. J. & Hayden, P. L. (1973) Studies on the hydrolysis and precipitation of aluminum(III). Columbus, Ohio State University. https://kb.osu.edu/server/api/core/bitstreams/3a36b3d7-33b1-5058-ae32-8e0a34fffa8e/content [Accessed: 16/01/2025].

Schmittinger, P., Florkiewicz, T., Curlin, L. C., Lüke, B., Scannell, R., Navin, T., … Bartsch, R. (2012) Chlorine. In: Ullmann's Encyclopedia of industrial chemistry, Vol. 8. Weinheim, Wiley. pp. 532–621. https://doi.org/10.1002/14356007.a06_399.pub3

Selin, H., Keane, S. E., Wang, S., Selin, N. E., Davis, K., & Bally, D. (2018) Linking science and policy to support the implementation of the Minamata Convention on Mercury. Ambio, Vol. 47. pp. 198–215. https://doi.org/10.1007/s13280-017-1003-x

Sola, I., Zarzo, D., Carratalá, A., Fernández-Torquemada, Y., de-la-Ossa-Carretero, J. A., Del-Pilar-Ruso, Y., & Sánchez-Lizaso, J. L. (2020) Review of the management of brine discharges in Spain. Ocean & Coastal Management, Vol. 196. e105301. https://doi.org/10.1016/j.ocecoaman.2020.105301

Song, Y. & Chen, C.-C. (2009) Symmetric electrolyte nonrandom two-liquid activity coefficient model. Industrial & Engineering Chemistry Research, Vol. 48. No. 16. pp. 7788–7797. https://doi.org/10.1021/ie9004578

Sraidi, A., Hak, S. A., Kounbach, S., Khaless, K., & Benhida, R. (2024) Extraction of rare earth elements using a chelating amino methyl phosphonic acid resin. Journal of Molecular Liquids, Vol. 402. e124758. https://doi.org/10.1016/j.molliq.2024.124758

Stringer, R. & Johnston, P. (2001) Chlorine and the environment: An overview of the chlorine industry. Berlin, Springer.
Tamás, B. B. (2021) Ioncserélő technológiák vizsgálata az elektrolízis sólevének tisztítására. Miskolc, Miskolci Egyetem (thesis work).
Titler, R. V. & Curry, P. (2011) Chemical analysis of major constituents and trace contaminants of rock salt. Pennsylvania Department of Environmental Protection, Bureau of Water Standards and Facility Regulation. https://files.dep.state.pa.us/Water/Wastewater%20Management/WastewaterPortalFiles/Rock%20Salt%20Paper%20final%20052711.pdf [Accessed: 22/04/2025].
Venkatesan, A. & Wankat, P. C. (2011) Simulation of ion exchange water softening pretreatment for reverse osmosis desalination of brackish water. Desalination, Vol. 271. No. 1–3. pp. 122–131. https://doi.org/10.1016/j.desal.2010.12.022
Virolainen, S., Wesselborg, T., Kaukinen, A., & Sainio, T. (2021) Removal of iron, aluminum, manganese and copper from leach solutions of lithium-ion battery waste using ion exchange. Hydrometallurgy, Vol. 202. e105602. https://doi.org/10.1016/j.hydromet.2021.105602
Vo, B. S. & Shallcross, D. C. (2003) Multi-component ion exchange equilibria prediction. Chemical Engineering Research and Design, Vol. 81. No. 10. pp. 1311–1322. https://doi.org/10.1205/026387603771339528
Wallace, P. S. (2015) System and method for removing minerals from a brine using electrodialysis. World Intellectual Property Organization International Bureau, Patent No. WO 2015/077,727 A1.
Wallace, P. S. (2021) System for removing minerals from a brine. US Patent No. US 10,954,150 B2.
Wang, S., Song, Y., Zhang, Y., & Chen, C.-C. (2022) Electrolyte thermodynamic models in Aspen process simulators and their applications. Industrial & Engineering Chemistry Research, Vol. 61. No. 42. pp. 15649–15660. https://doi.org/10.1021/acs.iecr.2c01881
Wong, T. C. & Dudeney, A. W. L. (1991) Ion exchange between solid phases: material balance and mechanism of interaction of aluminum hydroxide gel in aqueous suspension with a strong acid cation exchange resin. Hydrometallurgy, Vol. 27. No. 2. pp. 151–167. https://doi.org/10.1016/0304-386X(91)90063-R

Appendix

Characterization methods of ion exchange resins

The following parameters can be calculated based on the manufacturer's technical datasheets:

– External porosity (the ratio of the volume between resin particles to the total volume occupied by the resin bed):

$$\varepsilon_{out} = 1 - \frac{\rho_{bulk}}{\rho_{particle}}$$

– Pore volume of wet resin in the Na^+ form (V_{pore}, the volume inside resin particles per unit mass of resin): Since the pores of resins delivered in wet form are filled with water, the average pore volume of both resins is 0.6 cm^3/g based on moisture content, assuming the density of water is $\rho_{water} = 1\ g/cm^3$.

– Internal porosity:

$$\varepsilon_{in} = V_{pore} \cdot \rho_{particle}$$

– Solid density of the resin matrix in Na^+ form (ρ_{true}). The density of the resin particles in the wet state and their internal porosity (filled with water) are available, which allows for the following equation to be written:

$$\rho_{particle} \cdot V_{particle} = \rho_{water} \cdot \varepsilon_{in} \cdot V_{particle} + \rho_{true} \cdot (1-\varepsilon_{in}) \cdot V_{particle}$$

Expressed in terms of:

$$\rho_{true} = \frac{\rho_{particle} - \rho_{water} \cdot \varepsilon_{in}}{1-\varepsilon_{in}}$$

Certain parameters could only be determined by experimental measurements. These included the following:

– Volume reduction during $Na^+ \rightarrow H^+$ conversion: In this case, the manufacturer only provided an upper limit, but the actual conversion may be partial under pH 3 conditions based on the acid dissociation constants of aminomethylphosphonic acid *(Sraidi et al. 2024)*. To determine this, 10 mL of ion exchange resin in the Na^+ form (converted by shaking in NaOH solution) was shaken for one day in a pH 3 brine (25 wt% NaCl solution buffered to pH 3 with formic acid–sodium formate buffer), corresponding to the conditions of our pH optimization experiments. The resin volume was then measured.

– Average particle size (diameter) in the dry, H^+ form: The resin converted to the H^+ form as described above was dried, and the diameters of 20 individual resin beads were measured by electron microscopy and averaged.

– Average particle size (diameter) in the wet, H^+ form: For the European resin, the average particle size of wet resin beads in the Na^+ form was provided by the manufacturer. It was assumed that the relative volumetric reduction of a single resin bead (considered spherical) was equal to the volume reduction of the resin bed. Since the volume of similar objects scales with the cube of the similarity ratio, the change in bead diameter could be calculated based on the measured volume change, allowing the average bead diameter in the H^+ form to be estimated. For the Asian resin, it was assumed that the ratio between wet and dry bead diameters was the same as that of the European competitor. Using this ratio and the measured dry bead diameter, the wet bead diameter was calculated.

– Average particle size (diameter) in the wet, Na^+ form: This value was provided by the European manufacturer. For the Asian product, it was calculated using the previously determined wet H^+ form bead diameter and the similarity ratio derived from the measured volume change during $Na^+ \rightarrow H^+$ conversion.

– Particle density of wet resin in the H^+ form ($\rho'_{particle}$): Based on the resin capacity, the external porosity and the initially known particle density of wet resin in the Na^+ form, the final mass of a known volume (1 dm^3) of resin after replacing Na^+ ions with H^+ ions could be estimated from the difference in mass. The final volume of 1 dm^3 Na^+ form resin after conversion to the H^+ form could also be calculated from the measured volume change. The ratio of final mass to final volume yielded the particle density in the H^+ form.

– Solid density of the resin matrix in the H^+ form (ρ'_{true}): Assuming that the internal porosity does not depend on the ionic form of the resin, the solid density was

calculated analogously to the method used for the Na^+ form, based on the particle density and internal porosity:

$$\rho'_{true} = \frac{\rho'_{particle} - \rho_{water} \cdot \varepsilon_{in}}{1 - \varepsilon_{in}}$$

– Pore volume of wet resin in the H^+ form:

$$V'_{pore} = \frac{\varepsilon_{in}}{\rho'_{particle}}$$

– Specific surface area: The specific surface area was determined for the dry resin (previously converted to the H^+ form) using gas adsorption measurements and the BET method, expressed in m^2/g. Based on the diameter of a dry resin bead, its volume was calculated, and using the solid density of the resin, the mass of a single dry bead was obtained (assuming that the dry resin contains only the polymer matrix and air, with the mass of air being negligible). Multiplying this mass by the specific surface area (in m^2/g) yielded the surface area of a single dry resin bead. The average diameters of the dry and wet resin beads in the H^+ form allowed for the calculation of a similarity ratio between the two states. Since surface area scales with the square of this ratio, the surface area of a single wet H^+ form resin bead was calculated accordingly. The average volume of a wet H^+ form bead and the external porosity of the resin bed were then used to determine the bed volume corresponding to a single resin bead. Dividing the surface area of a single wet resin bead by this volume yielded the specific surface area of the resin with respect to bed volume, expressed in m^2/m^3. Alternatively, if the specific surface area is required relative to the mass of the wet H^+ form resin, it can be calculated as the ratio of the bead surface area to its mass (obtained from the product of its volume and density in the wet H^+ form).

Determination of the liquid-side overall mass transfer coefficient

The mass transfer is described by the following differential equations *(Cséfalvay et al. 2012: 390)*:

$$(1 - \varepsilon_{out}) \cdot \frac{d\bar{q}_{Al}}{dt} = a\beta_L \cdot (c_{Al} - c^*(\bar{q}_{Al})) =$$

$$= a\beta_R \cdot (q^*(c_{Al}) - \bar{q}_{Al}), \text{ where}$$

– ε_{out}: While typically referring to the external porosity of the resin bed, in this case, it represents the volume fraction of the liquid phase. This value accounts for the volume contraction between the Na^+ and H^+ forms of the resin, and also the fact that even in the initial 10 mL resin bed volume, a portion of the volume was occupied by liquid due to porosity.
– $\bar{q}_{Al}$: Instantaneous average concentration of aluminum in the resin phase, expressed in mol/dm^3.
– t: Time elapsed since the resin was added and shaking of the mixture was initiated.
– a: Specific surface area of the resin. It is traditionally expressed relative to the volume of the resin bed (m^2/m^3), but in the case of batch (shaking) experiments, it is expressed relative to the total volume of the reaction mixture.
– β_L: Liquid-side overall mass transfer coefficient, expressed in m/s.
– c_{Al}: Instantaneous concentration of aluminum in the liquid phase, expressed in mol/dm^3.
– $c^*(\bar{q}_{Al})$: Equilibrium aluminum concentration in the liquid phase that is in equilibrium with the instantaneous average composition of the resin phase, expressed in mol/dm^3.
– β_R: Resin-side overall mass transfer coefficient expressed in m/s.
– $q^*(c_{Al})$: Equilibrium aluminum concentration in the resin phase that is in equilibrium with the instantaneous average composition of the liquid phase, expressed in mol/dm^3.

Before solving the differential equation, the following assumptions and simplifications were made:

– Given that the total amount of aluminum in the liquid phase would only saturate approximately 0.1% of the total exchange capacity of the resin (based on our capacity measurements), the variation in the aluminum concentration in the resin phase can be considered negligible from the perspective of the driving force. Therefore, $\bar{q}_{Al}$ can be assumed to be effectively zero throughout the process in terms of its influence on the driving force (but the formula of the derivative is of course not constant). Consequently, the equilibrium liquid-phase concentration $c^*(\bar{q}_{Al})$, corresponding to this nearly zero resin-phase concentration, remains below the detection limit of both our photometric method and the ICP-AES measurements, and is therefore also taken to be zero.
– The liquid-phase aluminum concentration c_{A1} at each time point is directly calculated from the measured values (in ppm) using the molar mass of aluminum and the density of the solution. Based on the principle of mass conservation for aluminum ions, this enables calculation of $\bar{q}_{Al}$ in the resin phase.
– The liquid-side overall mass transfer coefficient β_L can be determined more directly than the resin-side coefficient. Since $c^*(\bar{q}_{Al})$ is assumed to be zero, the expression for β_L depends only on the time-dependent concentration profiles in each phase. Moreover, since the concentration of binding sites on the resin remains essentially constant (as only about 0.1% of them react during the process), the sorption kinetics can be treated as pseudo-first-order. (In contrast, calculation of the resin-side mass transfer coefficient β_R would require the time dependence of $q^*(c_{Al})$, which would need to be derived from the measured values of c_{Al} and our equilibrium data. However, identifying a suitable functional form for this dependence would require a

significantly more complex analysis.) Thus, the following appropriate kinetic equation can be fitted directly to the measured data:

$$c_{Al} = c_{0,Al} \cdot e^{-kt}$$
$$\bar{q}_{Al} = \bar{q}_{tot,Al} \cdot (1 - e^{-kt})$$

Here, k denotes the rate constant $(1/s)$, $c_{0,A1}$ is the initial aluminum concentration in the liquid phase, and $\bar{q}_{tot,Al}$ is the final aluminum concentration in the resin phase.

Since the concentration functions described above are differentiable and integrable, the differential equation can be solved. To do this, the variables are separated as follows:

$$(1 - \varepsilon_{out}) \cdot \frac{d\bar{q}_{Al}}{dt} = a\beta_L \cdot (c_{0,Al} \cdot e^{-kt} - 0)$$
$$(1 - \varepsilon_{out}) \cdot d\bar{q}_{Al} = a\beta_L c_{0,Al} \cdot e^{-kt} dt$$

By integrating both sides and factoring out constant terms:

$$(1 - \varepsilon_{out}) \cdot \int 1 \; d\bar{q}_{Al} = a\beta_L c_{0,Al} \int e^{-kt} dt$$
$$(1 - \varepsilon_{out})\bar{q}_{Al} = a\beta_L c_{0,Al} \cdot (-\frac{e^{-kt}}{k} + C),$$

where C is the constant of integration.

The value of C can be determined from the initial condition:

At $t = 0$, $\bar{q}_{Al} = 0$ (the resin is initially fully regenerated), hence

$C = 1/k$.

Substituting this back into the equation:

$$\bar{q}_{Al} = \frac{a\beta_L}{1-\varepsilon_{out}} \cdot c_{0,Al} \cdot \frac{1-e^{-kt}}{k}$$

Comparing this with the previous form:

$$\bar{q}_{Al} = \frac{a\beta_L}{1-\varepsilon_{out}} \cdot c_{0,Al} \cdot \frac{1-e^{-kt}}{k} = \bar{q}_{tot,Al} \cdot (1 - e^{-kt})$$

allows us to express the liquid-side overall mass transfer coefficient as:

$$\beta_L = \frac{\bar{q}_{tot,Al}}{c_{0,Al}} \cdot \frac{1-\varepsilon_{out}}{a} \cdot k$$

Based on this equation, the liquid-side overall mass transfer coefficient (β_L) can be calculated. The fitted kinetic curves are shown in *Figure A1*.

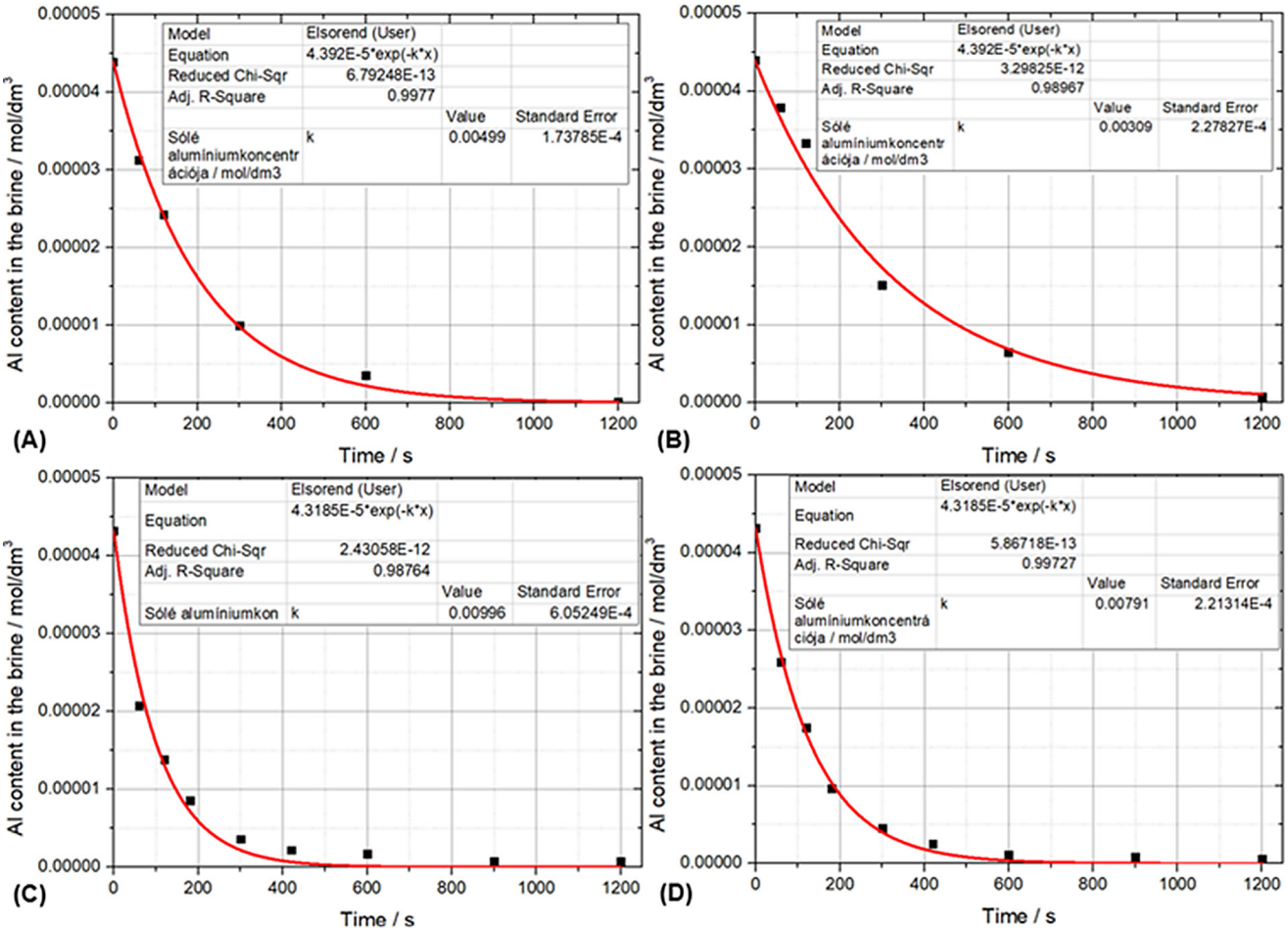

Figure A1 Fitting of pseudo-first-order kinetic curves to the experimental data points for the aminomethylphosphonic acid functionalized resin from the European (left: A, C) and the Asian (right: B, D) manufacturer at 20 °C (top: A, B) and 60 °C (bottom: C, D)

Source: Own work

Description of the ion exchange binding reaction using the Langmuir isotherm: curve fitting to experimental data

The appropriate curve fittings were performed for the Langmuir isotherm equation:

$$q = \frac{q_{max} \cdot K \cdot c}{1 + K \cdot c}$$

where q and c are the equilibrium concentrations of aluminum in the resin phase and liquid phase, respectively; q_{max} is the maximum binding capacity of the resin; and K is the equilibrium constant describing the binding reaction, serving as a fitting parameter. The fitted curves are shown in *Figure A2*.

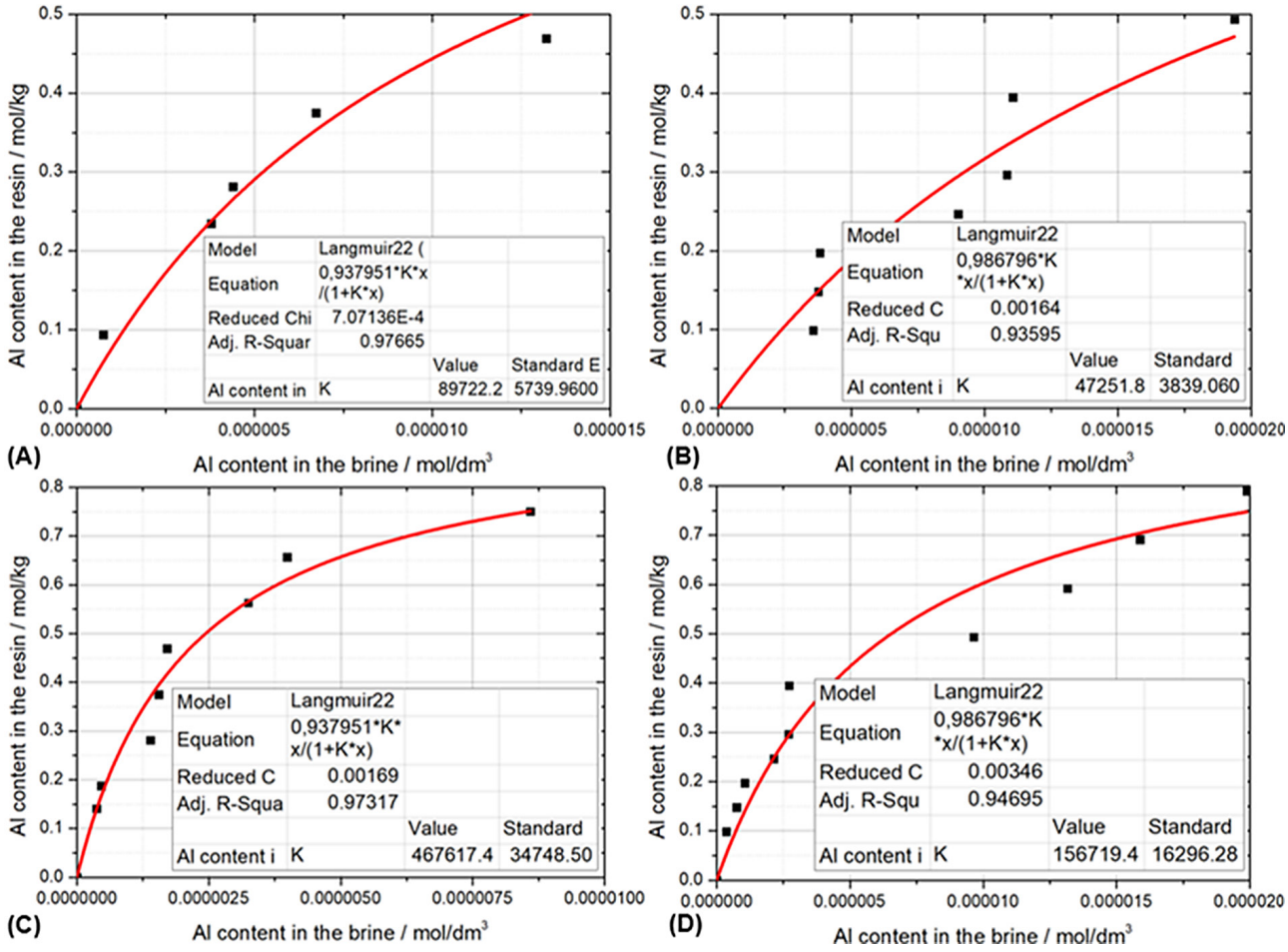

Figure A2 Langmuir isotherm curve fitting to the experimental data points for the European (left: A, C) and Asian (right: B, D) aminomethylphosphonic acid functionalized resins at 20 °C (top: A, B) and 60 °C (bottom: C, D)

Source: Own work